TECHNISCHE UNIVERSITÄT WIEN
Vienna University of Technology

Advancement of a mouse locomotion system based on X-Rays

DIPLOMA THESIS

submitted in partial fulfillment of the requirements for the degree of

Diplom-Ingenieurin

in

Biomedical Engineering

by

Anna Wolff, BSc
Registration Number 01426557

to the Faculty of Mathematics and Geoinformation

at the Vienna University of Technology

Advisor: Univ.-Prof. DDDr. Frank Rattay
Assistance: Prof. Dr. Elizabeth Brainerd, Brown University, RI, USA,

Vienna, 21st July, 2023

Anna Wolff

Frank Rattay

Acknowledgements

I would like to extend my sincere gratitude to Prof. Rattay for entrusting me with the opportunity to pursue my thesis abroad.
I am indebted to Prof. Brainerd, whose open and welcoming character made it possible for me to come to the United States. Without her willingness to take a chance on me, my dream of conducting research abroad would not have materialized. The collaborative atmosphere and inclusive environment you have cultivated within your lab have been instrumental in shaping my research and thesis. The camaraderie and support I have experienced by Elska, Hannah, Kelsey, Corrine and Erika have been incredibly invaluable and have allowed me to develop my skills and broaden my scientific horizons.
I would like to express my heartfelt appreciation to Alberto, whose exceptional technical expertise were vital to the analysis of my results. Moreover, I am incredibly grateful for your friendship. Your presence has been a constant source of support and encouragement and has shaped my stay at Brown immensely.
From the depths of my heart, I want to convey my gratitude to Leona, who has laid the groundwork for my thesis. Your work for the initial investigations has been immeasurable. Being my Uni companion since Day 1, I am so thankful for the friendship that has blossomed over this intensive and transformative time and feel so blessed to have you in my life.
In the face of the adversity I encountered last year with my battle against cancer, I am profoundly grateful to my parents, sisters, and brothers and friends for their unwavering support. Your love, strength, and encouragement have been my pillars of strength, giving me the courage to overcome challenges and pursue my dreams. I am immensely fortunate to have you in my life.
Embarking on my journey to the United States has been my greatest dream and I owe a debt of gratitude to my illness for teaching me the value of perseverance and the importance of seizing every opportunity.
Finally, I would like to express my gratitude to all the mice who have contributed to scientific research. Their sacrifice and the knowledge gained from their participation have been integral to the advancements in not only cancer research but numerous preclinical studies. Without their contribution, I would not be where I am today. Their invaluable role in furthering our understanding of medical science must be recognized and acknowledged.

Kurzfassung

Diese Arbeit bietet eine umfassende Diskussion über die Validierung eines X-Ray basierten Maus-Ganglabors für mögliche Anwendungen in präklinischen Studien. Der Schwerpunkt liegt auf der Analyse des Gangverhaltens von Mäusen und der Bewegung implantierter Marker mit dem Ziel, Erkenntnisse über Gangvariationen und die Auswirkungen von Schmerzen zu gewinnen. Das Ganglabor wird in Verbindung mit einem Schmerzmodell eingesetzt, um die Auswirkungen von Schmerzen auf Gangparameter zu untersuchen.

Der Validierungsprozess umfasst die Analyse des Mausverhaltens, um die Fortbewegungsmuster zu verstehen und das Gangsystem zu optimieren. Faktoren wie die Gewöhnung an die Umgebung und Gegebenheiten des Gang Systems werden untersucht, um flüssigere Bewegungen zu fördern und die motorische Leistung zu verbessern. Es wurde festgestellt, dass die Tageszeit das Aktivitätsniveau und die Gangstabilität beeinflusst, wobei tageszeitliche Schwankungen zu beobachten sind. Die Vorliebe von Mäusen für bestimmte Bereiche und ihre Abneigung gegenüber hell erleuchteten Umgebungen oder ihre Vorliebe für geschützte Räume werden ebenfalls diskutiert. Es werden Empfehlungen für die Erzielung eines stabilen Gangs bei weiblichen C57BL/6J-Mäusen gegeben, wobei Umweltfaktoren und die Aufrechterhaltung einer normalen Raumbeleuchtung berücksichtigt werden.

Die Analyse von Markerverschiebungen und Gelenkwinkeln wird mit Hilfe eines Arbeitsablaufs durchgeführt, der als Scientific Rotoscoping (SR) bekannt ist. Diese Technik ermöglicht die genaue Verfolgung und Analyse von Markerbewegungen im Verhältnis zu nahe gelegenen Knochen. Die Ergebnisse zeigen die Effektivität des SR-Arbeitsablaufs bei der Bereitstellung wertvoller Informationen über die Bewegungsmuster und Beziehungen zwischen implantierten Markern und Knochen. Trotz einiger Diskrepanzen zwischen dem realen Markerset und dem Knochenmarkerset trägt der SR-Arbeitsablauf zur Validierung des Ganglabors bei.

Anschließend wird das Schmerzmodell eingeführt, um die Auswirkungen von Schmerzen auf Gangparameter und Gelenkwinkel zu untersuchen. Gangparameter wie Schrittlänge, Schrittbreite und Schritthöhe werden analysiert und zeigen die individuelle Variabilität in der Reaktion auf das Schmerzmodell. Einige Probanden zeigen signifikante Veränderungen in diesen Parametern, andere hingegen nicht. Dies deutet darauf hin, dass die Auswirkungen von Schmerzen auf die Gangparameter nicht einheitlich sind und von individuellen Faktoren abhängen können. Es wird auch eine detaillierte Analyse der 3D-Gelenkwinkel durchgeführt, bei der die Bewegung der Markersätze zwischen

der Schmerz- und der Kontrollgruppe verglichen wird. Die Ergebnisse zeigen ähnliche Bewegungsmuster mit geringfügigen Unterschieden, was darauf hindeutet, dass das in der Studie verwendete Schmerzmodell die Gesamtbewegungsmuster der Hintergliedmaßen nicht wesentlich verändert.

Die Einschränkungen des Schmerzmodells, einschließlich der geringen Stichprobengröße und möglicher Störfaktoren, werden anerkannt. Die geringe Stichprobengröße kann die Feststellung eindeutiger Unterschiede in den Ergebnissen des Schmerzmodells behindert haben, und Störvariablen wie Schmerzintensität, -ort und -dauer können die Ergebnisse beeinflusst haben.

Zusammenfassend lässt sich sagen, dass diese Arbeit ein X-Ray basiertes Maus-Ganglabor erfolgreich validiert und wertvolle Einblicke in die Ganganalyse bei Mäusen, in Gangvariationen und in die Auswirkungen von Schmerzen auf Gangparameter liefert. Die Ergebnisse leisten einen Beitrag zur präklinischen Forschung und haben Auswirkungen auf die Untersuchung der Fortbewegung und auf Interventionen zur Verbesserung oder Wiederherstellung der Gangfunktion bei Mäusen. Künftige Studien könnten weitere räumlich-zeitliche Parameter untersuchen, andere mit dem Schmerz zusammenhängende Faktoren berücksichtigen und Längsschnittstudien mit größeren Stichproben umfassen, um ein umfassenderes Verständnis der Beziehung zwischen Schmerz und Gang zu gewinnen. Außerdem könnten Fortschritte in der microXROMM-Technologie die Analyse der Bewegungsdaten weiter verfeinern.

Abstract

This thesis provides a comprehensive discussion of the validation of an X-Ray based mouse gait laboratory for potential applications in preclinical studies. The focus is on analyzing mouse gait behavior and the movement of implanted markers with the goal of gaining insight into gait variations and the effects of pain. The gait laboratory is used in conjunction with a pain model to study the effects of pain on gait parameters.

The validation process includes analysis of mouse behavior to understand locomotion patterns and optimize the gait system. Factors such as environmental habituation and gait system conditions are examined to promote more steady movements and improve motor performance. Time of day has been found to influence activity levels and gait stability, with diurnal variations observed. The preference of mice for certain areas and their aversion to brightly lit environments or their preference for sheltered spaces are also discussed. Recommendations for achieving stable gait in female C57BL/6J mice are provided, taking into account environmental factors and maintenance of normal room lighting.

Analysis of marker displacements and joint angles will be performed using a workflow known as Scientific Rotoscoping (SR). This technique allows accurate tracking and analysis of marker motion relative to nearby bones. The results demonstrate the effectiveness of the SR workflow in providing valuable information about the motion patterns and relationships between implanted markers and bones. Despite some discrepancies between the real marker set and the bone marker set, the SR workflow contributes to the validation of the gait laboratory.

Then, the pain model is introduced to investigate the effects of pain on gait parameters and joint angles. Gait parameters such as stride length, step width, and step height are analyzed to show individual variability in response to the pain model. Some subjects show significant changes in these parameters while others do not. This suggests that the effects of pain on gait parameters are inconsistent and not uniform and may depend on individual factors. A detailed analysis of the 3D joint angles is also performed comparing the movement of the marker sets between the pain and control groups. The results show similar movement patterns with minor differences, suggesting that the pain model used in the study does not significantly alter the overall hindlimb movement patterns.

The limitations of the pain model, including the small sample size and potential confounders, are acknowledged. The small sample size may have hindered the detection of

clear differences in the results of the pain model, and confounding variables such as pain intensity, location, and duration may have influenced the results.

In summary, this work successfully validates an X-Ray based mouse gait laboratory and provides valuable insight into mouse gait analysis, gait variations, and the effects of pain on gait parameters. The results contribute to preclinical research and have implications for the study of locomotion and for interventions to improve or restore gait function in mice. Future studies could examine other spatiotemporal parameters, consider other factors related to pain, and include longitudinal studies with larger samples to gain a more comprehensive understanding of the relationship between pain and gait. In addition, advances in microXROMM technology could further refine the analysis of the movement data.

Contents

CHAPTER 1

Introduction

"Mice save lives". Rodents are the most extensively used research animals [Hickman et al., 2017]. Therefore, the skeletal kinematics of rats and mice are pertinent for research in the biomedical field, such as for preclinical studies, especially in the field of studies of illness models and pain. The purpose of this thesis is the further advancement of a standardized approach to analyzing the quantitative and qualitative gaits of rodents.

1.0.1 Importance of gait analysis in scientific research

Mice gait analysis is a powerful method for studying locomotor behavior and measuring different facets of motor control [Rizzi et al., 2023]: It involves the measurement and evaluation of mouse movements, particularly the coordination and timing of their limb placements during locomotion. Gait analysis provides quantitative data that can help researchers understand normal locomotion patterns, detect abnormalities, and investigate the effects of genetic, neurological, or pharmacological interventions on motor function.

Some of the many benefits of gait analysis include[Xu et al., 2019]:

- Disease simulation: Abnormalities in gait may point to a neuromuscular disorder. Researchers can learn more about the underlying disease mechanisms and potential therapeutic targets by analyzing gait in mouse models of human diseases.
- Drug development: Gait analysis is useful in drug development because it can be used to measure the benefits and drawbacks of different treatments. Researchers can use it to track any beneficial or detrimental effects that a drug has on their subjects' ability to move around.
- Functional assessment: Gait analysis can be used as a quantitative evaluation of motor function, making it a useful tool in functional assessment. It can be used by

scientists to monitor the development of diseases or the effectiveness of treatments, as well as to assess the functional recovery of patients following injuries or surgeries.

- Phenotyping: Researchers can use gait analysis to phenotype genetically modified mouse models of human diseases. Researchers can pinpoint the genetic changes that caused the abnormalities in gait by comparing the models' gait parameters to those of wild-type mice.

1.0.2 Pain as an applied example

The experience of pain in mice can cause behavioral changes, including abnormal gaits. Alterations in gait can be used to gauge pain levels or shed light on the causes of pain. An applied example would be the study of arthritis: Pain research using preclinical mouse models of arthritis benefits greatly from gait analysis [Jacobs et al., 2014]. This is because gait analysis can detect and quantify changes in walking patterns brought on by arthritis, such as limping or favoring one limb over the other. Researchers can evaluate the efficacy of arthritis therapies and interventions by studying gait patterns to assess the functional impairment induced by arthritis.

Gait analysis in mice is a useful method for studying locomotor behavior, evaluating motor coordination, and uncovering how environmental factors affect the way animals walk. It helps researchers learn more about normal and abnormal walking so they can create better treatments and interventions.

CHAPTER 2

Mouse Gait Analysis - State of the Art

There are a number of challenges that researchers in rodent gait laboratory must overcome before they can take reliable measurements. The following are examples of present problems and constraints: Rodent fur and loose skin are a significant obstacle to the establishment of a rodent gait laboratory because they hide the important joints and cause soft tissue motion artifacts [Kirkpatrick et al., 2022]. The shifting skeletal position in relation to the skin causes these artifacts to appear [Monsees et al., 2022]. Another problem is that rodents' crouching stance makes it harder to see the hip and knee joints, which are important for gait analysis. Despite improvements in visibility at the ankle joint, comprehensive measurement and visualization of 3D skeletal joint kinematics remains a difficulty in the rodent locomotion system [Brainerd et al., 2010]. Current rodent gait analysis systems require preceding training and tracking depends on the spatial resolution and accuracy of measurement methods [Xu et al., 2019]GaitSystems.

Methods for imaging and quantifying rodent gait are described in the following subsections, with an eye on their potential application in preclinical settings.

2.1 Gait analysis via paw print detection

CatWalk^{TM} (Noldus Inc., Netherlands) is a gait analysis system that consists of an enclosed walkway on a glass plate allowing a rodent to move from one side to the other [Xu et al., 2019]. Green light enters at the long edge of the plate and is completely internally reflected. Light is able to escape only at areas where the paws contact the glass plate, and the brightness of the scattered light is correlated with the contact intensity. The CatWalk^{TM} system includes a high-speed digital camera underneath the walkway with a sample rate of 100 frames per second. The camera lens has a diameter of 8.5 mm

and a curvature of 65°. The brightness of a pixel depends on the amount of light received from an area by the camera. However, the CatWalk^{TM} system faces some difficulties. One of the difficulties is that tracking is difficult but essential to avoid intensity signals from abdominal fur, especially in animals with severe pain. Another difficulty is that CatWalk^{TM} track lacks the ability to modulate track gradient and movement velocity. In gait analysis, velocity serves not only as a research result, but also as a factor causing considerable variability in other gait parameters.

DigiGait^{TM} (Mouse Specifics Inc., USA) and TreadScan^{TM} (CleverSys Inc., USA) are two additional rodent gait analysis methods in the paw print field; both use high-speed video cameras to capture the ventral view of rodent locomotion on transparent or translucent treadmills, and a running chamber to force the rodent into passive locomotion [Dorman et al., 2013]. The CatWalk^{TM} lets the rat walk or run at its own pace, while the treadmill method lets researchers manage its speed and position [Xu et al., 2019]. Figure 2.1 depicts the configuration differences between CatWalk^{TM} and DigiGait^{TM} (which is indicative of TreadScan^{TM}'s approach). Both DigiGait^{TM} and TreadScan^{TM} share CatWalk^{TM}'s drawback of providing inadequate data to serve as comprehensive rodent gait laboratories. Furthermore, there is a lack of consistency in the reproducibility of measurements made with these two systems (Abbas and Rodo, 2019).

Figure 2.1: Comparison CatWalk^{TM} and DigiGait^{TM}

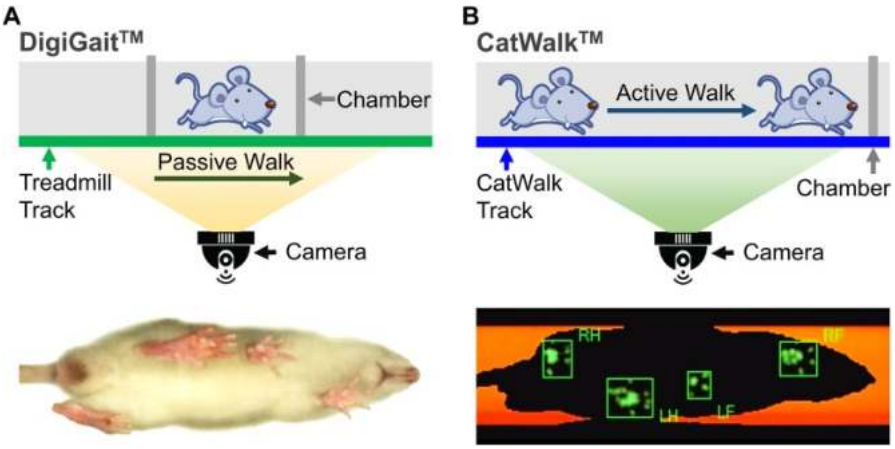

.

The mentioned methods are obviously insufficient for the visualization and quantification of limb kinematics in the sense of a rodent gait laboratory, but it is sufficient for the study of general gait patterns and the direct comparison of some parameters like step sequence and print position [Heinzel et al., 2020].

2.2 Gait analysis via external markers

Previously, rodent kinematics were observed and measured with the help of external markers [Wang et al., 2020]. After inducing a sciatic nerve crush injury in rats, a 3D motion capture system was employed to create a digital model of the injured limb in motion. In this research, adhesively placed external hemispheric skin markers were used to track the movement of the hind limbs. Since the rodents' skins were shaved before the marks were applied, the problem of fur artifacts was much reduced. The problem of inaccurately shifting loose skin remains, though. When compared to anatomical landmarks directly visible by X-ray methods [Bauman and Chang, 2010], these skin artifacts give inaccuracies of up to 39 degrees for knee rotation and 31 degrees for hip rotation in rats. In rodents, the ankle and foot region is less likely to create skin motion artifacts due to the less amount of fur and loose skin. However, there is an additional danger associated with externally marking these distal joints: the likelihood of rodent removal. .

Figure 2.2: (B) retroflective marker and (C) pen marker on rodent fur [Wong and Shah, 2019]

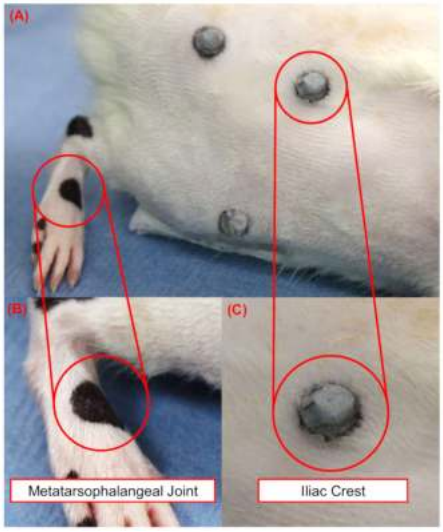

As depicted in Figure 2.2 [Wong and Shah, 2019], this issue can be addressed by using a mix of hemispheric external sticky markers and pen markers. However, the issue of skin motion artifacts exists since a precise assessment of the pen-marked joints' motions requires knowledge of their connection and relation to other joints' motions.

2.3 Gait analysis via for machine learning

Using the machine learning tool DeepLabCut is a viable strategy for addressing the drawbacks associated with the labor-intensive marker-less XROMM procedure (discussed

in greater depth in 4.1). High-speed biplanar X-ray movies of running rats were recorded for the purpose of this investigation [Kirkpatrick et al., 2022]. After carefully selecting skeletal landmarks for use in training a machine learning tool, DeepLabCut was able to generate 3D points that were within 2.4±0.2 mm of the accuracy of manually tagged sections. The root mean square error for 3D joint angles derived from both manually and automatically labeled landmarks was 0.33 degrees for the knee, 1.03 degrees for the hip, and 1.87 degrees for the ankle. However, unlike XROMM, this approach can significantly reduce analysis time without sacrificing accuracy. Researchers observed that after training DeepLabCut models, the labeling rate increased by a factor of 1627 compared to hand labeling [Kirkpatrick et al., 2022]. For usage in a standardized mouse gait laboratory, further work needs to be done, but this method offers a viable approach to automate the tracking process as part of the XROMM workflow, for example. This additional development would be simple for rats, as they weigh approxiamtely 300 gramm, but mice are 10 times smaller [Hickman et al., 2017], which presents new obstacles that weren't taken into account in the study. This research did not result in a mouse gait laboratory, but the machine learning component may one day prove useful in conjunction with the established methodology. Marker tracking in high-throughput research, in particular, may benefit from the supplied automation.

An additional machine learning strategy is provided by the research of Monsees et al. (2022)[Monsees et al., 2022], who created a videography-based method for quantifying the kinematics of freely moving rodents in their natural environments. This team of academics wanted to learn more about human decision-making by analyzing skeletal kinematics. To do this, scientists created a mathematical network model of the skeletons of mice and rats and applied anatomical restrictions to it. Then, for both objectives, a series of captured photos was used to manually track the 2D positions of markers painted to the animal's surface. The first involved training the machine learning program DeepLabCut, and the second involved fitting the 3D model skeleton to the anatomy of a specific animal. Using the 2D features captured by overhead cameras, DeepLabCut was trained to predict 3D poses of freely behaving animals [Monsees et al., 2022]. This method has the potential benefit of providing a quantitative analysis of mouse behavior free of artificial limitations. Kinematic quantification, however, relies on estimating poses by extrapolating bone-position data [Monsees et al., 2022]. While pose estimate of skeletal kinematics may be adequate for some uses, it cannot replace a mouse gait laboratory since it does not quantify bone positions directly as the animal behaves.

CHAPTER 3

Mouse locomotor behavior

Understanding mouse behavior is of paramount importance in the context of this thesis as it forms the foundation for investigating gait variations and the effects of pain.

3.1 Behavioral traits

Research into mouse behavior is an essential element of the neuroscience, biology, psychology, and animal behavior disciplines. Mice are commonly employed as research tools because of their adaptability as a model for human biology and behavior [Hickman et al., 2017]. They exhibit a wide variety of complicated and unique behaviors, from instinctual actions to higher-order cognitive ones like learning, memory, and decision-making. The discovery of innovative therapeutics for human diseases, as well as the general comprehension of many biological and psychological processes, relies heavily on the capacity to better understand mouse behavior. This thesis aims to investigate various aspects of mouse behavior, with the focus on locomotion, exploration, social behavior, and learning and memory.

Mice are sociable rodents that thrive in communal living situations. Pheromones are a major part of their communication system. There is a clear social hierarchy established through the use of olfactory signals [Hickman et al., 2017].

Mice, like other rodents, are nocturnal, meaning they are most active in the evening and early morning [Clark et al., 2006]. Mice exhibit thigmotactic behavior, often known as wall hugging, because they are a prey species [Hickman et al., 2017]. Because of the high risk of being captured by predators, they avoid open areas. For this reason, the experimental setup consisted of two enclosed and dark boxes that were linked together by a passage that was transparent. Mice, despite this, are naturally inquisitive and will investigate any novel items in their environment. They would cautiously peek outside of the boxes shortly after the gates were opened, and then travel through the tunnel towards

the other box. According to the findings of studies [Clark et al., 2006], mice usually start out their first walk in a hunched position, which is indicative of an exploratory behavior.

Mice have terrible eyesight and can't distinguish between colors. They use their acute hearing to sneak around undetected and their keen sense of smell and taste to find food. Mice can hear frequencies between 0.5 kHz and 120 kHz, with normal mice being especially attuned to sounds in the 12-24 kHz range [Hickman et al., 2017]. Due to the aforementioned reason, I was the only one conducting the experiments to accustom them to me and to reduce the amount of stress that would have been caused by several people, especially male persons [Sorge et al., 2014] observing the studies.

They can exhibit obsessive-compulsive behaviors, such as wire gnawing, circling, jumping, and hostility [Hickman et al., 2017], in response to specific environmental cues. These are some of the potentially stress-related, environment-related, or study-related behaviors that have been observed. The five mice were provided a place which increased the complexity of the habitat by using cardboard igloos and other structures such as nestlets and shredded paper as environmental enrichment and therefore supporting their natural hiding, burrowing and nesting behavior. Using enrichment gadgets and providing enough room and shelter for mice in the same cage moreover leads to less aggressiveness when housed together in groups [Hickman et al., 2017].

For the testing process, female mice rather than male mice were employed. The C57BL/6J strain of mice, produces female mice that are considerably smaller than their male counterparts. It is therefore more difficult to work with female mice; yet, doing so provides the opportunity to transfer procedures developed within this thesis with female mice to male mice, which is not necessarily the case when doing the reverse. It is important to keep in mind that different strains of mice exhibit very different responses to stress and behaviors similar to anxiety, although it is possible that other strains will prove to be adequate. A number of studies [Golden et al., 2011] that were recently conducted show that the C57BL/6J line, in comparison to other strains, appears to be more resistant to the effects of stress.

The objective was to train the mice to move continuously from one location to another without pausing, sniffing around, or hesitating at any point in their locomoting journey. Numerous tests with varying conditions were carried out in order to arrive at the most appropriate experimental design for the purpose of achieving this aim.

It was challenging to train them to walk in a particular way because of how easily they became diverted from the task. The use of this strategy demonstrates a straightforward and easy-to-replicate method for getting the mice to move from one box to the other. The findings of the tests demonstrate selecting a particular gateway and taking into consideration the various surrounding conditions to result in a re-createable environment for mice to move around in.

3.2 Evaluation of selected gait system

The Institutional Animal Care and Use Committee at the Brown University authorized all animal experimentation protocols, and all animals were cared for in accordance with NIH regulations. 5 female mice of the strain C57BL/6 were employed in this investigation. In order to reduce stress, the rodents were separated into cages containing three and two mice, respectively. Throughout the duration of the investigation, the temperature and humidity in each cage were kept constant. All of the mice in this study had unrestricted access to food and drink.

Behavioral testing was assessed for female C57BL/6 (n=5) mice. The length of the field of view of the X-ray equipment is 16 centimeters, and the challenge was to devise a method that would allow the mice to travel consistently within this area of view and complete an uninterrupted run.

The influence of contextual signals (both visual and room) on the motor activity of C57BL/6 mice was investigated in a series of experiments, with the following settings:

- The mice were acclimatized in the cages for thirty minutes, vs no acclimatization
- The light in the testing room was bright vs dimmed
- The height of the connecting section between the boxes was 2.5 inches vs 2 inches
- The mice would run back and forth vs doing a single run
- The experimental apparatus (boxes and tunnel) would be cleaned between each trial of mouse vs not
- The experiment was carried out in the morning (10am) vs in the evening (5pm)

It was noted down how many times stops occurred during 10 trials.

After capturing the mouse by its tail and placing her inside the box, the mouse would be acclimatized for 1.5 minutes. The gate would then be opened, and the mouse would begin to move towards the other box. The results indicate that this acclimatization period has a greater impact on their tendency to stop more frequently than not acclimating the mouse to the box and promptly opening the gate after transferring it to the box.

Under dimmed light, mimicking nocturnal state, mice made more stops than in trial that took place in a normally lit room. This thesis aims to develop a gait laboratory that is as simple as possible to be repeated by collaborators. Since many laboratories do not have a reversed day/night cycle, working at nocturnal would add a level of complication for conducting these experiments.

During the locomotion test, mice are prone to turning around more frequently when the tunnel is 2.5 inches in height. As a result, the tunnel was lowered by 0.5 inches, and the outcome indicated that they were less likely to halt and turn around during the trial.

Allowing the mouse to only run once and then removing her and replacing her with another mouse resulted in more stops per trial than letting the mouse run back and forth ten times. The first form of locomoting between the boxes was always in a hunched stance, which is normal and caused due to their inquisitive behavior. This slower, exploratory activity is then influenced by experience, and as a result, the mice got accustomed to the walking system with time, were more readily to explore in the beginning than after some runs.

Another experiment was to clean the gait apparatus between each mouse change. The result strongly indicate more stops for cleaning trials, versus no cleaning. Since cleaning also takes a considerable amount of time, it is advantageous that the mice halt more frequently when confronted with new scents, as opposed to their own or respective cage mates, which would have been in the same gait trackway previously. [Clark et al., 2006] shows that mice are most active very early in the morning or in the evening. The final setting of the experiment showed a similar result. A steady walk was needed and that occured more often at 10am in the morning than at 5pm in the evening.

Gait system

The gait system consists of of two acrylic boxes (5.1"x3.1"x4.1" LxWxH) and a connecting segment, a tunnel (21"x1.7"x4.1"). The acrylic material has a 1/8" width. The connecting tunnel can be inserted without any difficulty into any of the boxes' doors and is secured by its frame. The gait system rests on a styrofoam board, which is transparent for X-rays and readily transportable, allowing for an even gait.

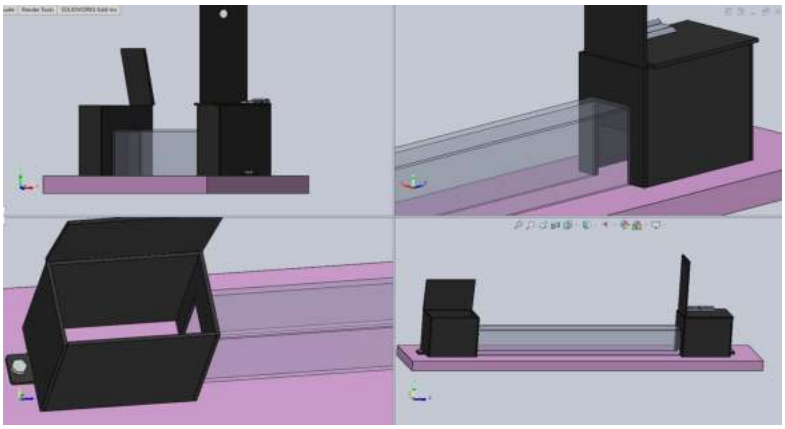

(a) Gait system

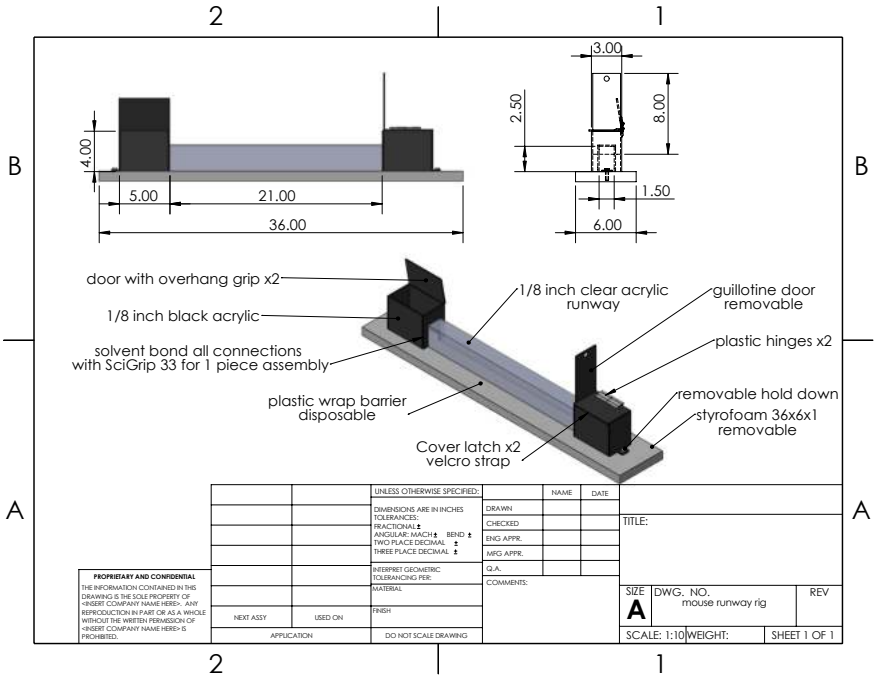

(b) trackway dimensions

Figure 3.1: The trackway consists of two boxes and a connecting tunnel

CHAPTER 4

Advancement of mouse gait analysis

Leona Loibl [Loibl, 2023] laid the groundwork for this gait development. I further advanced this gait analysis by examining the gait of a mouse while it was live-moving using the previously established and improved marker set. For its validation, the biomechanical analysis method XROMM was utilized, with a deeper focus on scientific rotoscoping (SR). The principal procedures and results are described in section 4.1. To evaluate the gait of mice, joint coordinate systems were utilized to derive gait parameters including joint angles, stride length, step width, and step height. In addition, a pain model was developed to assess differences in rodent gait.

4.1 XROMM

Loibl [Loibl, 2023] began the development of mouse gait analysis using microXROMM (small scale XROMM), a marker- and X-ray-based mouse gait analysis system.

XROMM (X-ray Reconstruction of Moving Morphology) [Brainerd et al., 2010] is a method that can be used to image and quantify the kinematics of movements in animals. This biomechanical analysis technique integrates dynamic high-speed X-Ray video fluoroscopy with static bone shape data from CT scans to image 3D limb kinematics in 3D space. XROMM can be differentiated into two main workflow types:

4.1.1 Marker-based XROMM

The marker-based XROMM is a highly invasive technique, because small radiopaque markers are surgically implanted into the bones. Full XROMM, which refers to a successful animation of the skeletal kinematics with six degrees of freedom, requires a minimum of three markers per bone. Due to the small scale of mice's bones, this surgery

is not feasible [Brainerd et al., 2010]. After markers are implanted, a biplanar fluoroscopy system [Brainerd et al., 2010] is used to record high-speed X-ray videos. The movies are then loaded into XMALab, a custom-made analysis program. There, the imaging volume is calibrated, and any distortions in the recorded images are corrected. Once 2D markers are selected manually in one frame, the software will automatically follow their positions throughout all recorded frames. A CT scan of the animal is performed alongside the procedures involving the X-ray motion data to see how the bone beads are settling into place. Open source medical imaging software Horos (The Horos Project, Horos v3.3.6) is used to extract polygonal mesh models of the relevant bones from the CT scan, and these are then loaded into the 3D computer graphics program Maya (Autodesk Inc., USA). The CT scan space XYZ marker coordinates are then calculated in Maya, and the X-ray space coordinates are transformed using a transformation matrix in XMALab. The two processes are integrated into one. After the bones have been moved, the data is sent back to Maya, where the polygonal mesh models of the bones are animated to provide genuine 3D motion in 3D space with six degrees of freedom.

4.1.2 Scientific Rotoscoping

Marker-free XROMM is an alternative to the invasive marker-based method [Gatesy et al., 2010]. Scientific rotoscoping is a manual registration process that combines bone shape data with X-ray motion data [Gatesy et al., 2010]. In the same way that marker-based XROMM generates anatomically accurate animations of 3D bone movement in 3D space with six degrees of freedom, markerless XROMM achieves the same [Gatesy et al., 2010].

The goal of SR (Scientific Rotoscoping) is to animate and quantify the skeletal movement of an animal using a 3D computer model. The process involves several steps:

- Recreating the Experimental Setup as a 3D Scene: The experimental setup, including components of the fluoroscopic imaging system and standard video cameras, is recreated as a 3D scene using animation software. Virtual cameras are calibrated to match the perspectives of the actual x-ray beam and standard cameras. Frames of video are displayed on background planes, which are viewed through each calibrated virtual camera.

- In this morphology-based approach, a digital marionette is built with movable virtual joints that may be independently manipulated. This way the registration is constrained by a key-lock-principle, with the anatomy representing the key and the X-ray video representing the lock. Creating the Digital Marionette: Polygonal models of relevant bones are created from CT scans of the subject. These bone models are articulated using virtual joints into a digital marionette. Virtual joints represent local coordinate systems that allow rotations and translations of one model relative to another. The virtual joints are configured to reproduce the rotations and translations of real joints in order to duplicate and quantify poses assumed by the skeleton.

- Registration and Animation: The digital marionette is posed by aligning each bone model to match the fluoroscopic and standard video backgrounds. Rotation and translation values for the model's degrees of freedom (DOF) are saved and graphed as a series of spline-interpolated curves. This process, known as registration, brings the 3D models into alignment with the 2D video. The marionette's DOF are adjusted over a sequence of frames to replicate in vivo poses, animating and quantifying the motion. The rotational and translational data can be exported for further analysis or integrated with the bone models to create rendered animations.

4.1.3 XMALab and XMAPortal

Both XMALab and XMAPortal are integral parts of the XROMM process. After obtaining the high-speed video files used in biplane fluoroscopy, as well as the files used to calibrate and correct for distortion, the data is submitted to XMAPortal (Xray Motion Analysis Portal, [www.xmaportal.org]. The XROMM data formats, including X-ray videos, calibration images, and CT scan data, may all be efficiently managed thanks to XMAPortal. It has a number of useful functions, such as the ability to tag uploaded files with metadata or to selectively or publicly share data with others. Compressing high-speed films to JPGs is another useful feature because it facilitates quicker and simpler analysis.

The X-ray data analysis program is XMALab, which was developed specifically for the XROMM project [Knorlein et al., 2016]. It is used to monitor the marker beads in both perspectives in 2D space and incorporates the calibration, distortion correction, and animal movement photos. It also enables the generation of rigid bodies with known joint motions, and the subsequent export of this joint motion data to Maya for use in animating the bone CT scans.

4.1.4 X-Ray imaging components

The accumulation of high-speed X-ray fluoroscopy videos is an integral part of the refined mouse gait laboratory. In order to better grasp the topics discussed later, a brief overview of the various components of a standard X-ray fluoroscopy setup is provided. The kilovolt peak (kVp) and tube current (mA) that are given to the X-ray tube are primarily controlled by the X-ray generator [Schueler, 2000]. Both continuous and pulsed modes of operation are possible for the generator, with the latter offering superior temporal resolution. The main primary X-ray settings are kVp (kilovoltage peak), the peak voltage difference between the cathode and anode and the amount of current (in milliamperes mA) [Schueler, 2000] that flows through the tube. The X-ray tube is responsible for transforming the electrical energy from the X-ray generator into an X-ray beam [Schueler, 2000]. The tungsten wire filament that serves as the cathode in this unit releases electrons when heated, and these electrons are drawn to the copper anode [Schueler, 2000]. Focal spot refers to the point on the anode where the electrodes make contact. Distance from the focal spot at the source to the object being imaged is

known as the source-object distance (SOD), whereas the distance from the focal spot at the source to the image receptor is known as the source-image distance (SID). The collimator, essentially a set of radiopaque shutter blades, is the next building piece, and it is responsible for regulating the size and form of the X-ray beam. This collimation also improves visual contrast by decreasing scattered radiation [Schueler, 2000]. Beam hardening effects are mitigated by passing the collimated X-ray through a copper or aluminum filter. These low-energy X-rays increase the dose to the subject without significantly bettering the quality of the image.

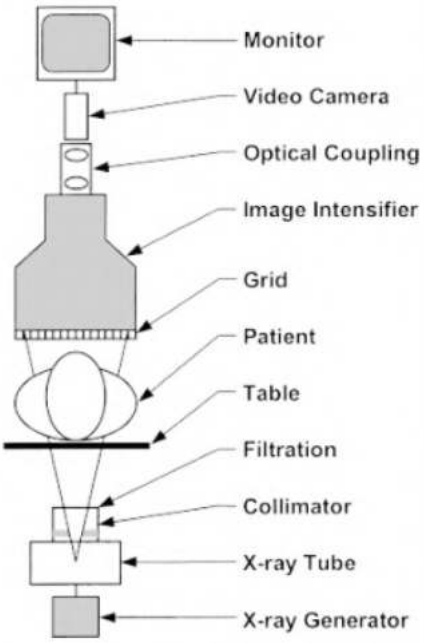

Figure 4.1: Fluoroscopic imaging elements [Schueler, 2000]

Minimizing the attenuation of the X-ray beam by the table is necessary if the configuration shown in the image is employed. Figure 4.1 shows a human patient, but for this study, a mouse is used instead. The grid lets only X-rays traveling in the right direction through to the image intensifier, which increases contrast. By transforming the X-rays into visible light photons, the image intensifier (II) transforms the X-ray beam energy into a real-time image. In order to transport an image from an image intensifier to a video camera, an optical coupling device is required. Images captured by a camera are displayed on a screen, which can be connected to further software for analysis.

4.1.5 Marker set

In order to track the mouse's locomotion, radiodense markers were injected into their hindlimbs. The development of this set of markers, was done by my colleague Leona Loibl [Loibl, 2023], and is briefly described in the following paragraph. As described in

2.2, skin motion artifacts can cause inaccuracies of up to 39 degrees when using external skin markers [Bauman and Chang, 2010]. Therefore, rather than utilizing externally applied markers, spherical tantalum beads with a diameter of 0.26 mm were injected percutaneously into the mice's soft tissue. In order to create a functional mouse gait laboratory, it was decided that the animation should represent the foot, tibia, femur, and pelvis. These were the primary targets for the injected marker set, and all of them went through the validation procedure described in Chapter 5.1. Alongside this primary requirement lay the goals of selecting marker placements and creating injection procedures that are both repeatable and reasonably straightforward to master for future application and use by collaborators.

Marker requirements

Tantalum beads with a diameter of 257.9 μm were used as markers (Bal-tec, USA). In this thesis, the diameter was rounded to 0.26 mm (260 m) for convenience. Symbolized by the letter Ta and with the atomic number 73, tantalum is a pure metal with several beneficial medical applications [Mani et al., 2022]. The radiopaqueness of tantalum is the most crucial quality for this project and other X-ray related studies since it makes the beads easily visible in the high-speed X-ray videos and microCT scans that are obtained. Ceramic beads have been investigated as a less costly alternative to tantalum beads. Unfortunately, these beads ranged in size from 0.21 to 0.25 μm. The ceramic beads did not generate any abnormalities on the CT scans, but due to their non uniform diameter, the tantalum beads were preferred.

Marker locations

Literature review on mouse anatomy [Colville and Bassert, 2016] provided the foundation for selecting optimal injection sites for the radiopaque tantalum beads in the mouse body tissue; additional criteria included the palatability of characteristic anatomical landmarks and the repeatability of the injection technique per site. After perfecting the injection process, the best location for each marker was identified and used as a target for future injections. Each marker was labeled and numbered to distinguish them. Table 4.1 lists the marker names and numbers and describes their placement. In order to establish joint coordinate systems, two additional beads were added to Loibl's [Loibl, 2023] marker set, explained in more detail in 5.1.1.

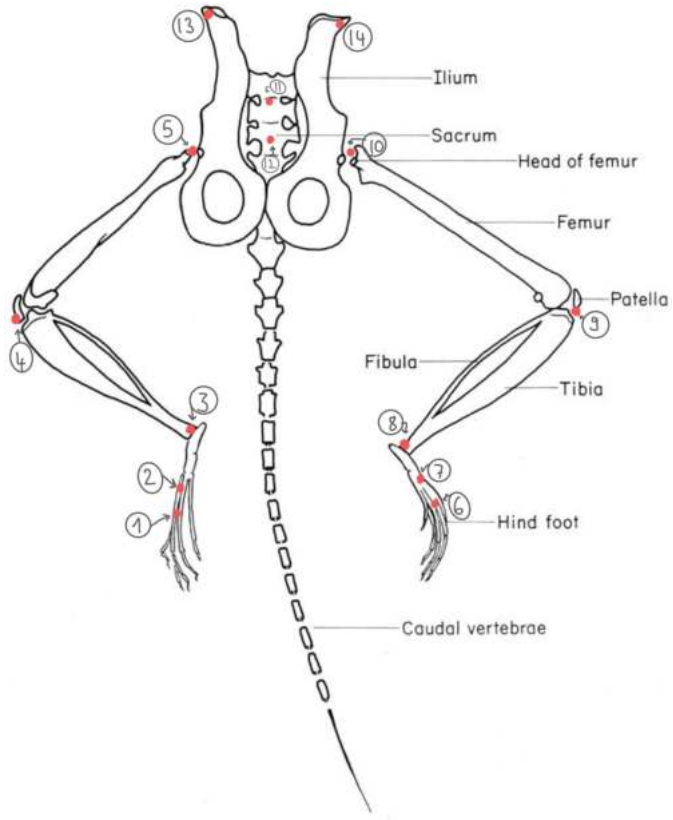

Figure 4.2: *Mus muculus* anatomy of the pelvic and hindlimb [Cook, 1965]

Left distal foot	1	Distal end of third metatarsal
Left proximal foot	2	Proximal end of third metatarsal
Left ankle	3	Lateral malleolus
Left knee	4	Deep to the patellar tendon
Left hip	5	Between head of femur and greater trochanter
Right distal foot	6	Identical to left side
Right proximal foot	7	Identical to left side
Right ankle	8	Identical to left side
Right knee	9	Identical to left side
Right hip	10	Identical to left side
Pelvis cranial	11	On sacrum between illia, ca. 1cm caudal to illiac crests
Pelvis caudal	12	On caudal spine between illia, ca. 0.5cm caudal to Marker 11
Left illiac crest	13	On tip of left illiac crest
Right illiac crest	14	On tip of right illiac crest

Table 4.1: Implanted marker set

4.1.6 Marker implantation workflow

5 female mice of the strain C57BL/6J were chosen for this thesis' gait analyis. Female mice were purposefully chosen since they are more difficult to work with due to their smaller size. This was done so that the procedure could be easily transferable to male mice. Mice were given isoflurane at a concentration of 3% in an induction chamber with an oxygen flow rate of 0.8 l/min. After the mouse had stopped moving, the chamber was slightly tilted to test for the oresence of the animal's righting response. Once this was confirmed, the mouse was placed in a nasal cone and given a 2% isoflurane as a maintenance anesthetic. Ophtalmic ointment was put in the eyes to avoid the cornea from drying out. After the hindlimbs were shaved, their ears were punched to identify them.

To facilitate access to various injection sites, the mouse was put in a sterile environment and supported on a foam structure. To ensure that the mice were kept warm, a heating pad was placed under the sterile drape. All tools used in the procedure had been autoclaved or were packaged under sterile conditions. To guarantee a smooth procedure, the mice's respiration rates regularly monitored. The mice had their reflexes measured before, during, and after the treatment using the toe pinch method. A 23-gauge hypodermic needle was used to inject marker beads one at a time into the soft tissure until the needle's tip was in the right spot. The markers were then carefully expelled from the needle's tip using a surgical wire plunger. The marker injection procedure required a "helper", who was responsible for holding the mouses' limbs in place, allowing the injector easy access to the injection site. A nonsteroidal anti-inflammatory analgesic, Meloxicam (2 mg/kg), was given to the mice after surgery, and an analgesic, Buprenorphine sustained-release (Bup - SR), 0.5 mg/kg, was given to the mice before surgery. The Institutional Animal Care and Use Committee (IACUC) of Brown University gave their consent to all of the methods used.

CT scan

After the injection procedures, the mouse was scanned with a microCT scanner (Bruker SkyScan 1276, Belgium). The animal was put in a cassette and the inbuilt anesthetic delivery via an internal pump allowed for in vivo specimen scanning. The mouse's front teeth were put into the tooth hook within the animal cassette to ensure proper alignment for obtaining anaesthetic and for consistent scans. The specimen was kept anesthetized using a nasal cone and live camera footage within the Bruker SkyScan 1276 program allowed to monitor the mouse breath. With the scanning parameters described below in table 4.2, a 3 minute scan was ensured so to save on anesthetic costs while still achieving high enough quality for subsequent mesh model segmentation.

Filter	kV	mA	Resolution
Al 0,5 mm	65 kV	200	5k

Table 4.2: microCT scaning parameters

As Loibl [Loibl, 2023] demonstrated in her thesis that the healing phase into embedding tissue takes one week, the five mice recovered for two weeks to ensure complete healing of the markers.

4.1.7 muXROMM workflow

After the healing period of two weeks, the established gait analysis was conducted. The created marker set was validated throughout the specimen's motion to ensure its use in future gait analyses. The following section guides through the steps involved in retrieving the mouse locomotion data.

Locomotion data acquisition

Whenever locomoting experiments were conducted on the specimen, it was necessary to provide a dark environment to ensure active state. Therefore, whenever the mice were transported, for instance to the X-Ray room, their cage was concealed by a drape.

To ensure safety, Brown University's Department of Envrionmental Health and Safety requires every individual working with X-Ray equipment to complete its radiation machine safety training course. The mouse handling operator must wear a radiation dosimeter, which retrieves information about the radiation being exposed to during the procedure and a radiation badge that aggregates all radiation exposures acquired during the span of the project in order to comply with radiation safety measures. To further enhance safety from X-Rays throughout the radiology process, a lead apron and lead collar is worn.

Once the X-Ray perspective, as explained in chapter 4.1.8 was set up, a metal grid with circular perforations and known distances between these holes was adhered to each of the image intensifiers and imaged. Using this image and the idealized geometry of the undistortion grid, the fluorscopes' distortion is later corrected in the XMALab tracking process. The foam platform was placed on a lifting platform and pushed into the X-Ray system using brick blocks. The foam construction allowed for placement adjustments as necessary, which conveniently facilitated the increase or decrease of the SOD. Foam's near-transparency to X-rays makes it an ideal construction material, as it won't interfere with a moving specimen. A Small Lego Cube, as described in section 4.1.8 was placed on the foam platform and imaged for the 3D geometry calibration of the imaging system. Then, the X-Ray system was ready to capture the images of the mouses's locomotion. The X-Ray assistant altered the X-Ray parameters, as described in section 4.1.8 and the gait system was placed on the foam platform. The gait system was positioned inside the X-ray machine so that the tunnel's center fell within the X-ray's 16cm field of view.

A specimen was taken out of its cage and placed inside the gait system box. Reduced stress levels were guaranteed after a 3 minute acclimation period. The mouse handling operator then opened the gate and moved as far away from the X-Ray source as feasible while still being able to see the mouse's stride through the gait system. The mouse handler would shout "go" whenever the rodent was ready to leave its cage and cross to the other side, at which point the X-ray technician would begin taking images. Ten

separate trials were recorded of each specimen. A successful trial is only a trial, in which the mouse locomotes to the other box without stopping in the field of view. All trials in which the mouse stopped during moving to the other box were excluded and deleted from the platform. Following these 10 trials, the gait system was disinfected with non-alocholic wipes to remove any lingering odors. The mice were returned to their mouse chamber, after each underwent 10 trials.

The X-Ray files were subsequently exported as AVI files on a hard drive and uploaded on XMAPortal. XMAPortal converts the AVI files to JPG files, which can be consequently downloaded and analyzed in the XMALab software.

XMALab tracking

In the marker tracking process in XMALab, as explained in section 4.1.3, the first step was to upload the X-ray videos to XMAPortal, where they were compressed to JPG format for easier analysis and improved efficiency. The compressed images were then analyzed in XMALab, starting with correcting the image distortion caused by the fluoroscopes. The 3D space was calibrated using the Small Lego Cube as the calibration object. All 14 markers, were tracked using XMALab's automatic tracking feature, with manual adjustments when necessary. The markers were tracked frame by frame using the algorithm's built-in automatic marker tracking capability, with some modifications made by hand for markers in positions that the program had trouble recognizing. To ensure minimal marker overlapping during the tracking procedure, the optimal X-Ray perspective had to be determined, explained in more detail in section 4.1.8.

Exporting Coordinates

Data on the markers' 3D motion in X-ray space was exported from XMALab as a comma-separated values (CSV) file. A MatLab script was written specifically for this gait's analysis, in more detail in chapter 5.1.1. This script involves parameter calculations such as gait components including stride length, step width and steph height, but also joint angles such as abduction and adduction and flexion and extension produced by the hindlimbs. The finished product of the mouse gait laboratory are these gait parameters. The gait parameters resulting from the MatLab analysis were consequentially compared to the bone movements, simulated by scientific rotoscoping. The workflow to obtain the bone movements vie scientific rotoscoping is explained in the following chapter.

4.1.8 microXROMM settings

Previous settings

The development of microXROMM played a crucial part in Loibl's work [Mani et al., 2022]. It aimed to improve the precision of XROMM, a modified X-ray system used to capture high-speed X-ray videos of animal behaviors. While the existing system could accurately capture larger animals, such as dogs and macaques, mice posed a challenge due to their

small size and fast movements. To address this, the X-ray system and subject setup were optimized to increase tracking precision from ±0.1 mm to ±0.02 mm, enabling the imaging of small-scale animals like mice. This enhanced workflow, combining improved X-ray images with microCT scans, was referred to as microXROMM or muXROMM. The high-speed X-ray videos of mice obtained through microXROMM were crucial for validating the developed method through full marker-based microXROMM. The optimization process involved adjusting parameters such as magnification, source-object distance, and focal spot size, with the goal of finding the best combinations to enhance imaging quality. The experiments used mouse cadavers with marker beads and involved static and dynamic imaging. The results showed that higher magnification led to increased precision, achieved through magnification modes and positional magnification. The choice of magnification level also influenced the focal spot size and imaging volume. Visual comparison of the X-ray images led to the selection of optimal settings, including magnification mode level 3 and a close distance of 30 cm to the image intensifiers. These settings enabled tracking of the marker beads with higher precision. Overall, the modifications in the imaging technique resulted in a precision of ±0.02 mm, paving the way for microXROMM.

Adjusted and optimized settings

This thesis project required varied parameters due to the nature of the object being studied. Even though a higher magnification mode led to increased precision, the image was too dark. To track the marker in XMALab, the picture needs to be at a certain brightness and for this reason a reduced magnification option (magnification mode 2) was needed. Due to the mouse's diminutive stature, a small focal spot size was necessary. Changing the kV parameters produced two different effects: The first one focuses on how bright the X-Ray photons are, while the second one analyzes how energetic they are.The contrast of the image is altered as a result of this. In general, a lower kV will produce a higher quality image contrast. However, in order to ensure that there is sufficient brightness, having enough kV is also essential. Following several rounds of trial and error, the following configurations were decided upon: The images were recorded at continuous mode at 72kV (camera 1) and 68kV (camera 2), with 100 mA and an exposure time of 500 μs. Due to the rapid mouse locomotion movements, the sample rate was 200 frames per second.

Compression and calibration settings for XROMM

In the XROMM workflow, there are two stages where compression options can be applied to the X-ray footage. The first stage is when exporting the X-ray image files from the camera's hard drive, and the second stage is when converting AVI files to JPG files using the XMAPortal platform. Loibl [Loibl, 2023] conducted a compression test to learn how compression affects bead tracking accuracy and to devise a process that maximizes compression without sacrificing accuracy. The accuracy of the marker tracking was evaluated by filming high-speed X-rays of a loon cadaver bone with implanted beads. The results showed that the differences in accuracy between the three compression

methods were minimal, and double compression (FFmpeg compressed JPGs generated by XMAPortal from the H.264 compressed AVIs) was selected due to its time savings.

In the calibration process for X-ray acquisition, Loibl [Loibl, 2023] compared two calibration objects to evaluate their influence on tracking precision. The "Small Acrylic Cube," is made up of three thinner acrylic sheets and 48 beads of the same size and shape. The second item, aptly dubbed the "Small Lego Cube," is constructed from LEGO® bricks that have had beads pressed into the openings. The same X-ray video with distortion correction was used to study both objects. Both items are similarly exact, as there were only small changes in the marker tracking precision across the calibration procedures. Lego cubes are easy to assemble and reproduce, however acrylic cubes are better for use with external cameras because to their transparency. The Small Lego Cube was subsequently employed in X-ray experiments, as well as in the mouse gait laboratory, because no external cameras were used in the research.

Validation of X-Ray perspective

The reality that different anatomic structures overlap each other can make imaging a body a challenging task at times. By supplying diagnostic images, the technologist plays a critical part in ensuring that the diagnosis is as accurate as possible. As a result, a technologist needs to be familiar with the many different positions and procedures that are necessary in order to isolating and providing a clearer view of a bodily part that is being imaged. In addition to improving one's ability to view a particular anatomical structure, different projections also help adjusting the field of view. Two distinct points of view were compared and contrasted with the assistance of Professor Brainerd's knowledge and experience gained over the course of many years:

The lateral oblique and dorsal oblique perspective with two different directions of the trackway: transversal and longitudinal directions.

First set-up as shown in Figure 4.3: Lateral oblique perspective.

For the lateral image acquisiton of the mouses' gait, the image intensifiers and X-Ray generators are placed in an 45 degree angle lateral to the animal. The X-Rays cross the trackway in an 90 degree angle in the horizontal dimension. The machines are properly aligned and the center of the X-Ray beams cross each other in the same distance.

Examining an X-ray frame in which the animal is moving through the same phase of its gait cycle allowed for a comparison to be made between the various orientations.

Both Figures 4.4a and 4.4b demonstrate that there is an overlap of the markers at the ankle and proximal foot during the swing cycle. As a consequence, the XMALab computer software will no longer perform automatic marker tracking, and the crosshairs of the markers will need to be specified manually instead. In XMALab, the monitoring of the marker was halted 15 times, in both the left and right of the figure 4.6.

Outcome for the lateral oblique perspective: The transversal direction is limiting the field of view, as less steps are received compared to the longitudinal direction.

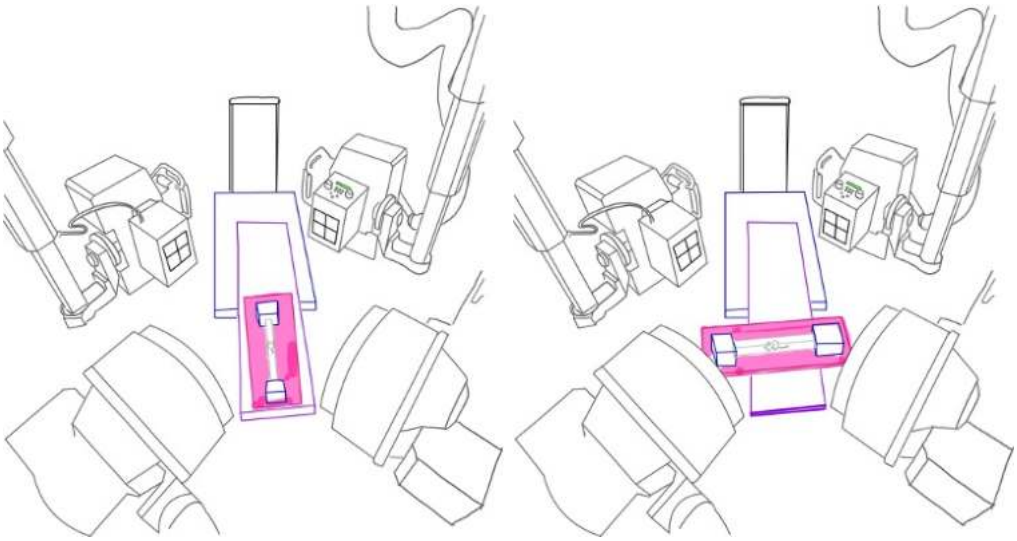

(a) Lateral longitudinal (b) Lateral transversal

Figure 4.3: The lateral oblique perspective with the trackway in two different directions

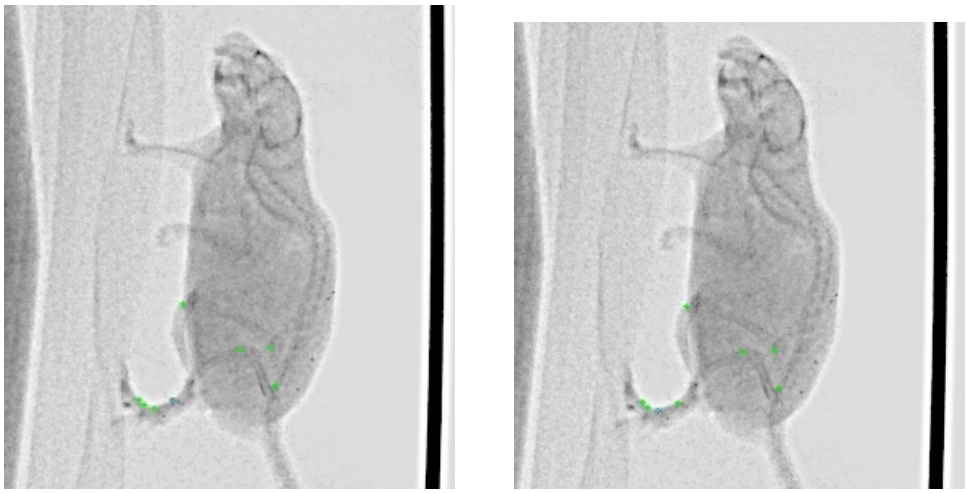

(a) Lateral longitudinal 21 (b) Lateral transversal 18

Figure 4.4: Swing-phase of a mouse walking in longitudinal and transversal direction in the lateral oblique perspective

Second set-up as shown in Figure 4.5: Dorsal/ventral oblique perspective.

The anterior-posterior oblique view requires the image intensifiers and X-Ray generators to be obliquely positioned 45 degrees dorsal to the animal in the vertical dimension. The X-Rays cross the trackway in an 45 degree angle.

The dorsal oblique transversal perspective 4.6b is not an optimal match for the tracking

of the markers as 41 separate occasions resulted in the monitoring having to be corrected manually. Sometimes the marker would cease moving while the proximal foot bead was in the swing phase, which caused a blurring with the ankle bead and the distal foot bead of the same foot. This happened when the foot was in the swing phase. There were instances when the marker did not stand out sufficiently. Because of motion blur and the rapid movement of the feet, this X-Ray perspective is not appropriate for the trackway alignment in question because it makes the pictures less distinguishable from one another.

The dorsal oblique longitudinal 4.6a on the other hand turns out to be an excellent fit. Without any overlaps and therefore causing no disruptions it automatically marker monitors the gait of the mouse, making this the most convenient view to work with.

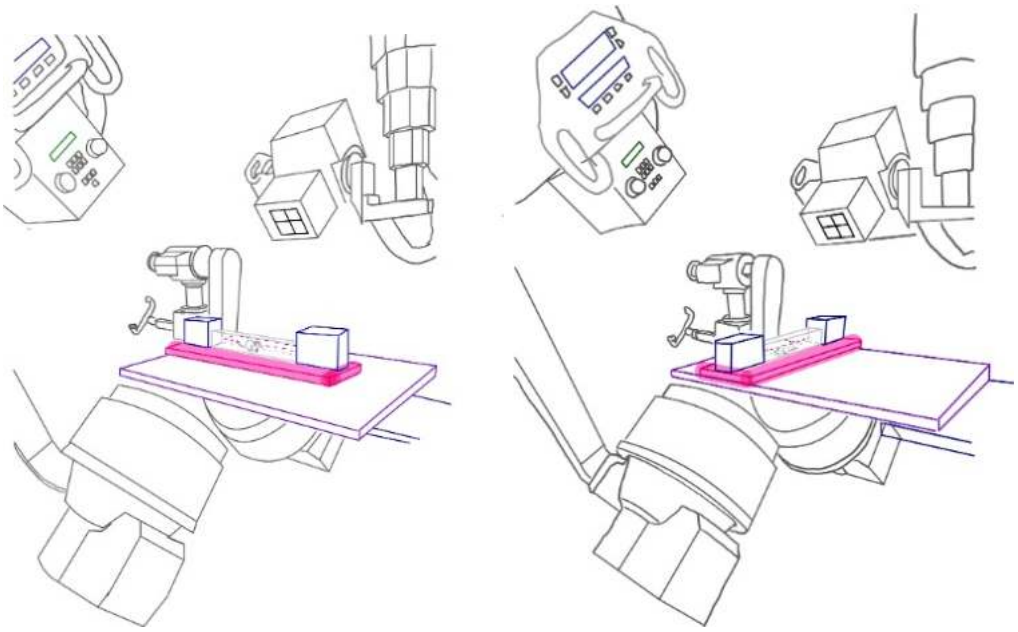

(a) Dorsal longitudinal (b) Dorsal transversal

Figure 4.5: The dorsal oblique perspective with the trackway in two different directions

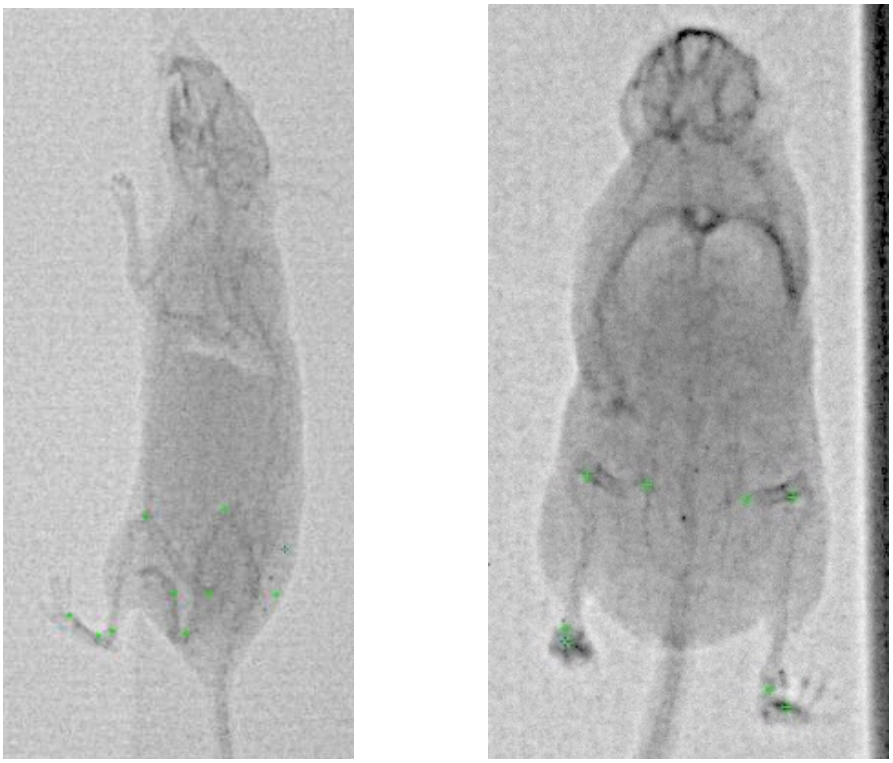

(a) Dorsal longitudinal 6 (b) Dorsal transversal 14

Figure 4.6: Swing-phase of a mouse walking in longitudinal and transversal direction in the dorsal oblique perspective

4.1.9 SR workflow to obtain results if beads are moving during live locomotion

As Loibl [Loibl, 2023] showed in her thesis, the implanted markers were remaining in place over time. The developed marker set shows negligible little motion artifact relative to the bones in a puppeted dead mouse. In order to validate this thesis' gait analysis, it was important to know if the beads are moving relative to the bones during natural locomotion in a live mouse. In order to obtain these bone kinematics, the scientific rotoscoping method was used.

As explained in section 4.1.2, the process involves several steps. Firstly the X-Ray videos of the live locomotion had to be obtained. For that Mouse Nr. 04 was chosen. A marker set as desrcibed in 4.1 was implanted, followed by a recovery period of two weeks. After getting the XYZ coordinates of its movements, using the microXROMM method described in 4.1.7, the mouse was humanely euthanized, according to Brown University's IACUC protocols. The mouse with the injected soft tissue markers was scanned using the microCT scanner.

microCT scan

Since scan time is less of an issue with a mouse cadaver than with living mice, the settings were adjusted to generate a considerably higher quality scan. A source voltage of 45 kV and a source current of 200 umA were used to scan the mouse cadaver. The Al 0.25mm filter used produced a scan that took 24 minutes. The resulting DICOM data was then used to obtain the hindlimb bone objects.

Bone mesh models segmentation

The 3D Slicer software [www.slicer.org] was used to convert image sequence from JPGs into nrrds. To segment bone mesh models, the rigid bodies pelvis, femur, lower leg and foot were created using this software and the corresponding bone markers. Bones were separated from other tissues by allocating a certain thresholf of bone density and creating areas of interest (ROI) on each slice that included the bones and bone markers while excluding soft tissue and the injected soft tissue marker set. The marker set beads were left out so that they could be animated independently, reflecting their actual movement rather than an illusionary connection to the bones. Although interpolation between slides was possible, the ROIs were produced by hand for the most part. More manual tweaking was required for areas that required more precise segmentation, such as joint interfaces, such as the patella of the knee and the head of the femur. After refining the view to include only the necessary details of the mesh model, the individual bones of interest were exported one by one as OBJ mesh model files. Importing the bone mesh models and the marker mesh models that corresponded to them into Maya was the next stage; there, the starburst artifacts brought on by the radiodensity of the marker beads were smoothed out without altering the skeleton's real anatomical structure.

Animation and registration

In this part of the scientific rotoscoping process, the XYZ marker coordinates in 3D microCT space are initially generated in Maya after importing the bone marker mesh models. To replicate in-vivo poses, a joint marionette was created to position the rigid bodies. This joint marionette was semi-automatically rotoscoped by matching the bones to their respective X-Ray shadows every 10 frames. A rotoscoping rig enabled a pelvis system with the acetabula staying affixed to femoral head. The rotation and translation of the femur and lower leg limbs, as well as the foot were matched independently in every 10th frame (resulting in 50 frames over the course of the video). These hindlimb degrees of freedom were saved and interpolation between these keyframes led to a smooth, dynamic movement of the marionette. This process, known as registration brings the 3D models into alignment with the 2D videos.

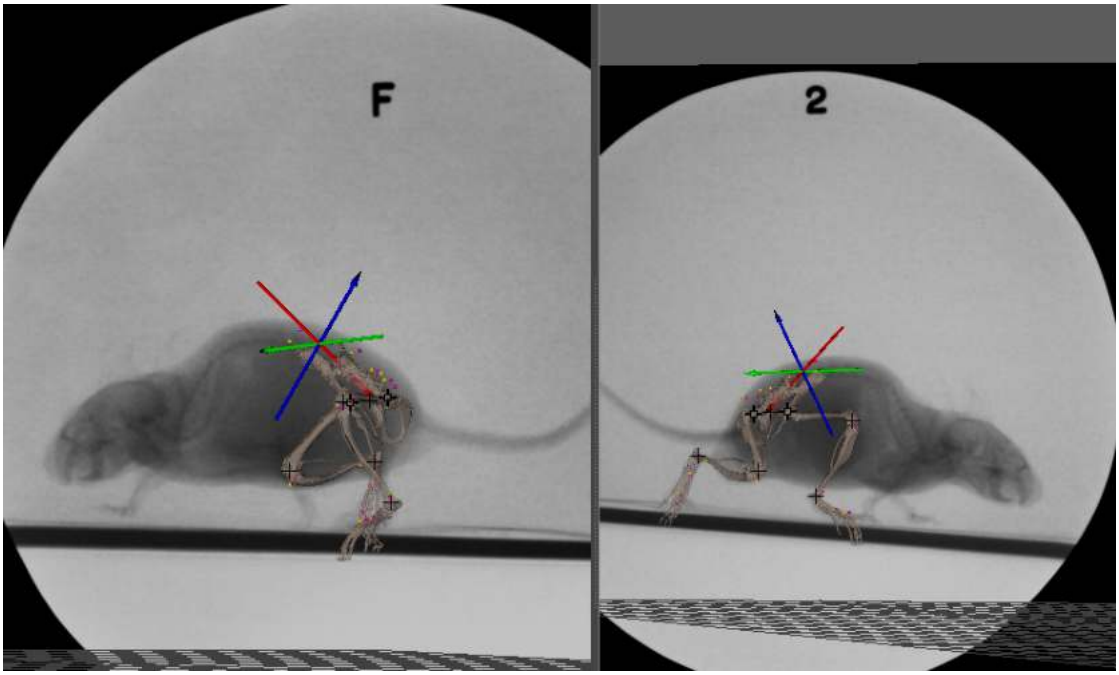

Figure 4.7: Scientific rotoscoping registration: alignment of 3D bone models to 2D videos

Movement of beads compared to bones

Following the rotoscoping phase, the main goal was to determine the degree of displacement that beads in the soft tissue showed in relation to the nearby bones. To achieve this, the XYZ coordinates obtained from the tracking process of the μXROMM workflow were imported into the Maya software. Subsequently, a procedure known as "baking" was executed within Maya. The baking process eliminates hierarchical structures within an animation, resulting in the animation of individual objects being "baked" into their respective properties, mimicking a manual animation of each bone.

Within a selected frame, the markers were duplicated onto the bones, thereby generating a "bone marker set" that remains attached to the bones throughout the entire locomotion sequence. Consequently, as shown in figure 4.7, two distinct marker sets coexisted within the locomotion sequence: a yellow marker set, which remained rigidly affixed to the bones, and a pink marker set representing the actual markers that were surgically implanted into the soft tissue, exhibiting movement relative to the bones.

To determine the magnitude of displacement between the implanted marker set (pink) and the bones (yellow), both marker sets were exported. Subsequently, an Excel file was developed to facilitate the analysis of their movements.

CHAPTER 5

3D joint angles

5.1 Evaluating gait

To validate the established gait development, gait patterns among the 5 specimen were analysed in the following section. Investigating the differences in rodent gait can shed light on the intrinsic and environmental factors that influence locomotor behavior. By quantifying and comparing the gait patterns of various mice, it is possible to obtain a thorough understanding of the inter- and intra-individual differences in their locomotor characteristics.

To measure gait parameters, a MatLab script was created. This allowed to define orientations and measure angles relative to the local axes of the joint, providing insights into joint movements and kinematics.

5.1.1 Joint coordinate systems

The first step in obtaining specific gait data was the establishment of a joint coordinate system throughout the mouse's hindlimbs.

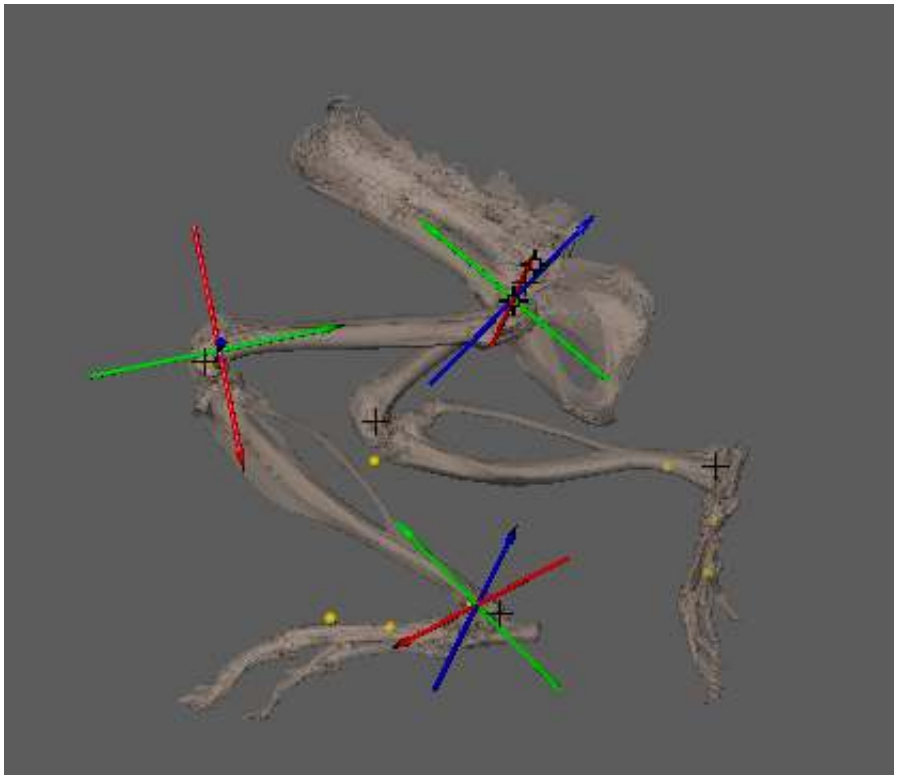

Figure 5.1: Joint coordinate systems in hip, knee and ankle

To calculate joint angles, such as flexion & extension, abduction & adduction of the hip and flexion & extension of the knee, as well as flexion & extension of the foot, joint coordinate system were created in hip, knee and ankle, as to be seen in figure 5.1. Due to the symmetry of the mice hindlimbs and the injected marker set, the validated joint coordinate systems of hip, knee and ankle are representative for both sides. Every joint was defined by three mutually orthogonal vectors. These vectors are referred to as the X-axis (red), Y-axis (green) and Z-axis (blue) of the joint's coordinate system.

To define the coordinate systems in the left joints, the markers from the established gait analysis were used as landmarks. The coordinate system on the left hip was defined as follows:

- Y-Axis (green) is the vector pointing from left hip joint to the left illiac crest marker.
- X-Axis$*$ (red) represents the direction from left hip joint to right hip joint.
- Z-Axis (blue) is the result of the crossproduct from normalized Y- and X-axis.

The true X-Axis is calculated as the cross product of normalized Y-Axis and Z-Axis, ensuring that all three vectors form a right-handed coordinate system.

The process for defining the coordinate system for the left knee followed a similar approach:

- Y-Axis (green) points from left knee joint to left hip joint.
- X-Axis∗ (red) represents the direction from left knee joint to left ankle joint.
- Z-Axis (blue) is the result of the crossproduct of the normalized Y- and X-axis.

The true X-Axis is calculated as the cross product of the normalized Y-Axis and Z-Axis, ensuring a right-handed coordinate system.

Similar as the above mentioned coordinate systems, the JCS on the left ankle was defined as follows:

- Y-Axis (green) is the vector pointing from left ankle joint to left knee joint.
- X-Axis∗ (red) represents the direction from left ankle joint to left foot marker.
- Z-Axis (blue) is the result of the crossproduct of the normalized Y- and X-axis.

Finally, the true X-Axis is calculated as the cross product of the normalized Y-Axis and Z-Axis, ensuring a right-handed coordinate system.

Equivalently, the coordinate systems on the right side were created.

To analyze gait parameters, such as step height or stride length, another coordinate system needed to be created to serve as a body coordinate system, depicted in figure 5.2.

- Y-Axis (green) is the locomotion direction of the mouse, representing the cranial-caudal axis.
- X-Axis∗ (red) is obtained by subtracting the right illiac crest marker from the left illiac crest marker.
- Z-Axis (blue) is the result of the crossproduct of the normalized Y- and X-axis.

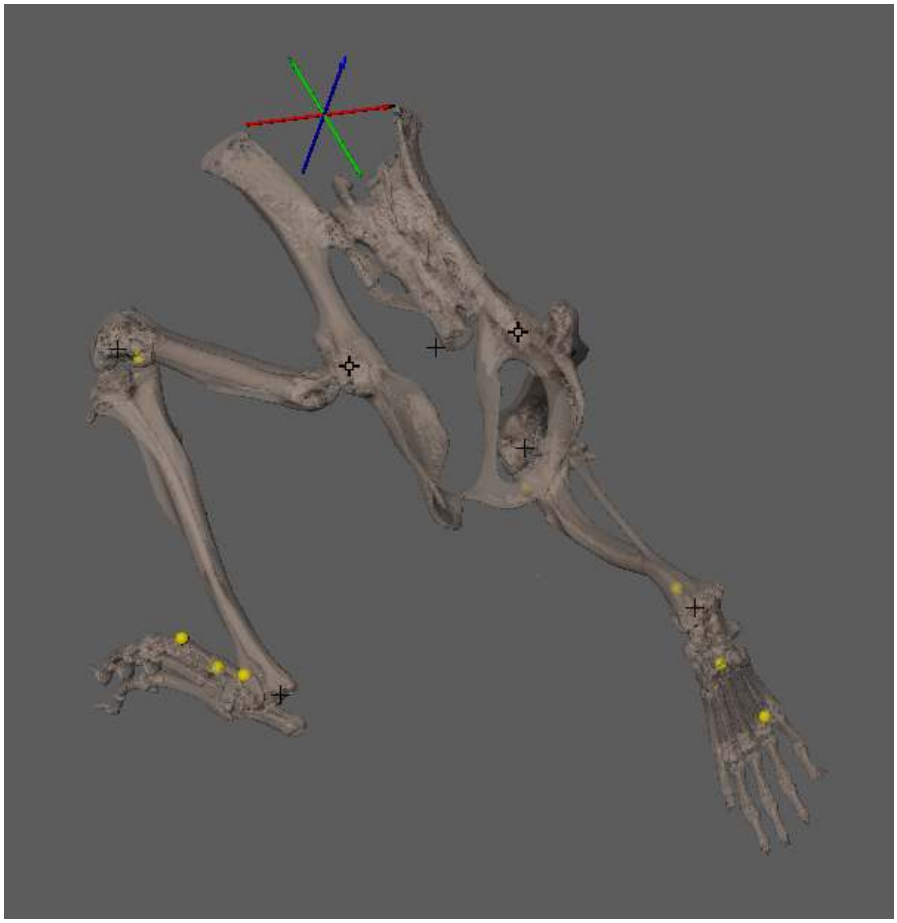

Figure 5.2: Body coordinate system

5.1.2 Derivation of 3D angles

The accurate measurement and analysis of joint angles are crucial for understanding movement dynamics.

To determine the precise joint angles of flexion and extension in the hip and knee joints, as well as the angles of abduction and adduction in the hip joint, the MatLab script employed a quaternion multiplication approach and coordinate system transformations.

The first step involved defining local coordinate systems for each joint of interest, namely the hip (left and right), knee (left and right), ankle (left and right), and foot (left and right). These local coordinate systems were established with respect to a global coordinate system in section 5.1.1. The coordinate system vectors were derived using cross products and normalization operations. These vectors represent the axes of the local coordinate systems.

Next, the joint data points were transformed to their respective local coordinate systems.

This transformation involved projecting the joint data onto the local coordinate system axes using dot product calculations. This step allowed for the representation of joint movements in the local coordinate systems, facilitating subsequent angle calculations.

To calculate the flexion and extension angles of the hip and knee joints, quaternion multiplication was employed. Quaternion multiplication combines rotations around specific axes to yield the final rotated angles. For flexion and extension, the target axis was set as the local Z-Axis (representing flexion/extension movement), while the local X-Axis was set to 0. This configuration ensured that the rotations occurred within the desired plane of movement.

Similarly, quaternion multiplication was also employed to determine the abduction and adduction angles of the hip joint. The quaternion multiplication formula was applied, but this time, the target axis was set as the local X-Axis (representing abduction/adduction movement), while the local Z-axis was set to 0. This arrangement enabled rotations within the desired plane of movement.

Once the quaternion multiplications were performed, the resulting rotated vectors were obtained. These vectors represented the joint orientations after the flexion, extension, abduction, and adduction rotations. The angles were then derived from the rotated vectors using appropriate trigonometric functions, such as arctangent.

The same approach was applied to the right hip and knee joints to calculate the corresponding angles. By utilizing quaternion multiplication and the change of coordinate system, the script successfully derived the flexion and extension angles in the hip and knee joints, as well as the abduction and adduction angles in the hip joint, providing valuable insights into the joint movements during the analyzed motion.

CHAPTER 6

Pain model

Abnormal gaits are one of the behavioral alterations observed [Dorman et al., 2013] after mice feel pain. To implement this thesis's established gait analysis, a pain model was applied and subsequent gait parameters were evaluated and compared to a control trial. This mouse procedure was carried out in accordance with the National Institute of Health guidelines and approved by the Institutional Animal Care and Use Committee (IACUC) of Brown University.

6.1 Pain model workflow

The pain model's workflow can be summarized as follows: To start, a 3-millimeter deep and 5 mm long incision was made in the left hind limb's skin and muscle. Afterwards, the mouse's nociceptiveness to pain is evaluated using the von Frey test. Approximately two hours, after the surger, mouse locomotion was recorded and tracked as detailed in the ref*mu*XROMM workflow. Ten trials were conducted on each mouse. Following Brown's IACUC protocol, the mice were humanely euthanized 6 hours after the surgery. Lastly, the pain model's tracked data was compared with the control model. The same mice used in the pain model had their locomotions monitored and recorded for the control model two weeks prior. For this, the same amount of trials was recorded to ensure a direkt comparison with the pain model.

6.2 Hind paw incision model

Among various pain models, the hind paw incision model was chosen because it is a well-established experimental technique that is highly reproducible and used commonly in clinical research. Both skin and muscle incisions are necessary in this mouse model for postoperative discomfort. Very acute pain is most accurately simulated by incision of both skin and muscle, as in invasive surgery.

Surgery procedure

To initiate the procedure, the mice are prepared by allowing them to acclimate to the laboratory environment, reducing stress levels and ensuring their overall health. Anesthesia is then administered to the mice by putting them into an induction chamber and giving them isoflurane at a concentration of 3% with an oxygen flow rate of 0.8 l/min. To test for righting reflexes, the chamber was slightly tilted. While the assistant performed the proper anesthesia on the mouse, the surgeon got sterile. For that, sterile surgical procedures were followed. The After confirming a no-response reflex, the mouse was transferred to a sterile drape and her head was placed into the nose cone and given a 2.7% maintenance anesthetic. The mouse was covered by a piece of Press and Seal wrap, except for the left hind paw designated for the operation. The translucent press and seal wrap allowed for continuous monitoring during surgery. Once the left hind paw was taped down with surgical tape and secured, a cotton swab of 75% ethanol followed by a new cotton swab of betadine was applied. These applications were repeated three times. Continuous checks to see if the mouse was fully anesthetized were performed by pinching the medial toe. If the mouse was flinching, the anesthetics was increased to 3% concentration. With a stainless steel No. 11 surgical blade, an incision through the skin and fascia was made from 2mm from the proximal edge of the heel to 5mm down towards the toes in the center of the hind paw. This first incision was followed by a second longitudinal, 3mm deep cut through the muscle. The wound was closed by putting two sutures in the skin approximately 3mm apart using a 6-0 silk suture. If bleeding occurred during the procedure, cotton swabs were applied with pressure until the bleeding stopped. After a short recovery period of 1.5 minutes from the anesthesia, the mouse was placed back into her cage, which sat on a heating pad to ensure a warm environment.

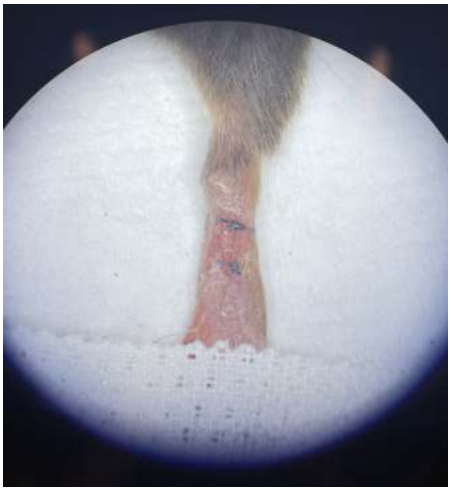

Figure 6.1: Suture of hind paw incision

6.2.1 von Frey

There are different options to determine pain perception [Modi et al., 2023]. For this thesis, the von Frey method was chosen, due to its simple and non-invasive nature and the ability to allow for comparisons between different types of groups, such as control and pain experimental group. Unlike some other pain assessment methods that involve invasive procedures, such as nerve stimulation or surgical interventions, the von Frey test does not cause tissue damage or significant distress to the animal. It is a straight-forward procedure that can be easily performed with minimal training and equipment.

To measure the pain sensitivity induced by the paw incision, the Electronic von Frey apparatus (Ugo Basile® Dynamic Plantar Aesthesiometer 37450) was used. It provides a quantitative assessment of mechanical allodynia and hyperalgesia, which are conditions characterized by heightened sensitivity to normally non-painful stimuli or increased sensitivity to painful stimuli, respectively.

The mechanical threshold of the mouse hind paw was measured by exposing the mouse to a metal wire mesh table in a plastic box. Prior the start of the von Frey analysis, the mouse was habituated to the clear boxes for 30 minutes. The apparatus was sealed off with dark plates by each side to decrease stress, created by the bright illuminated room and the experimenter moving around the room. The dynamic plantar aesthesiometer (Ugo Basile Cat. No. 37450), an automated testing instrument, applied a mechanical stimulus to the plantar surface of the hind paw from below the bottom of the test room. With the help of a tilted mirror, attached to the testing instrument, it was possible to visually detect the foot paws and move easily from testing animal to testing animal. Over the course of 30 seconds, a force ranging from 0 to 5g was applied to the back paw at a rate of 0.16 g/s using a steel rod with a diameter of 0.5 mm. As soon as the animal removed its hind paw, the mechanical stimulus ceased, and the force with which the paw was removed was recorded to within 0.1 g. Animals were subjected to five consecutive trials with at least 5 min between the trials.

(a) Ugo Basile® Dynamic Plantar Aesthesiometer 37450

(b) force application on hind paw by steel rod

Figure 6.2: von Frey testing

.

6.3 Mouse gait

Assessing gait measures is crucial for studying gait alterations in for instance OA models [Jacobs et al., 2014] due to the intersection of biology and mechanics in the disease. Two different characteristics were examined in this gait analysis: Spatial gait data and temporal characteristics. Spatial gait data describe the geometric characteristics of a footprint pattern, including parameters such as stride length, step width, and step height. Stride length represents the distance between two foot strikes of the same limb, while step length describes the limb's forward distance relative to the contralateral limb.

Temporal data in gait analysis refers to the timing and synchronicity of foot-strike and toe-off events. The gait cycle, as depicted in figure 6.3, reduced to a repeatable sequence normalized by stride time, is classically represented by a Hildebrand plot [Jacobs et al., 2014]. Temporal variables derived from the gait cycle, such as limb duty factor, temporal symmetry, and limb phase, are critical in understanding foot-strikes and toe-off events in quadrupedal gait sequences. Limb duty factor, also known as limb percentage stance time, represents the percentage of time a limb is in ground contact. Together with temporal symmetry and limb phase, these variables provide insights into the sequence of events during locomotion.

Gait cycle

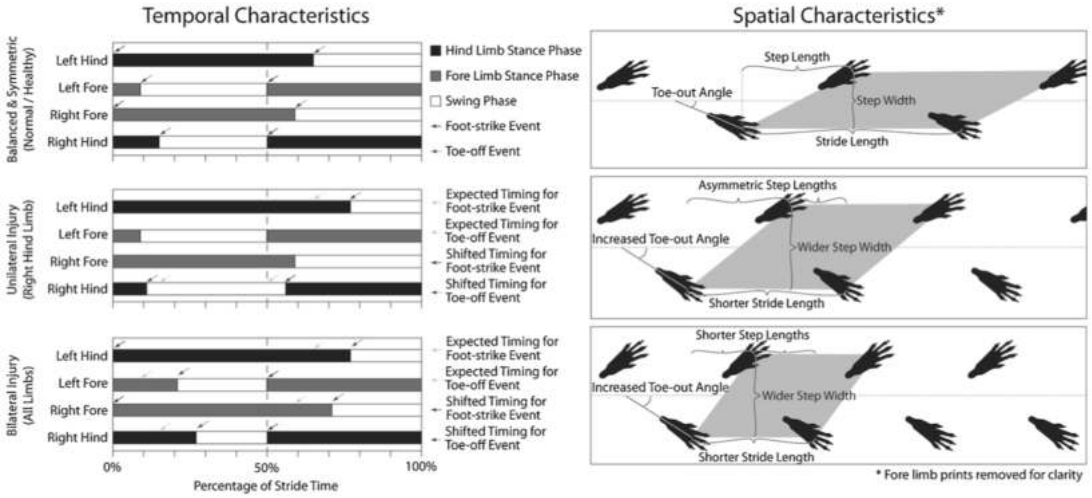

Figure 6.3: Rodent gait cycle[Jacobs et al., 2014]

Two consecutive left-hind foot-strikes comprise a gait cycle, and temporal variables specify the timing of each foot-strike and toe-off in that cycle. The white bars represent a limb's forward translation, while the black bars represent a limb's stance, which is the amount of time it is in contact with the ground. The solid arrows indicate the beginning of the stance, and the dotted arrows indicate the beginning of the swing. Foot-strikes on the

left and right (fore and hind) limbs of a rodent's gait are roughly equally spaced in time (step length is about 50% stride length) and in space (step length is about 50% stride length). The rodent gait is typically symmetrical, with equal amounts of time spent on the left and right limbs (fore or hind).

Possible unilateral injury gait alterations

As in Jacobs et al. [Jacobs et al., 2014] paper described, uneven and asymmetrical walking patterns may result from a single-sided injury. This paper proposes that single-sided injury leads to a widened step width, a shortened stride length and step height and asymmetry in right and left limb step lengths. Stance time on the injured limb (right hind in this example) may also decrease, and the temporal gait pattern becomes asymmetric (right hind foot-strike occurs after 50% of gait cycle).

6.4 Gait parameters

Stride length

Stride length is the distance between two foot strikes of the same limb.

$$\boldsymbol{Stridelength} = \|foot_{left}(2) - foot_{left}(1)\|\vec{e_x}$$

When the animal is walking in a straight line, the stride lengths must be approximately equal and will not vary between limbs [Jacobs et al., 2014].

Step width

Step width refers to the distance between the left and right paws during gait.

$$\boldsymbol{Stepwidth} = \|foot_{left}(1) - foot_{right}(1)\|\vec{e_y}$$

Step height

Step height is the vertical distance traveled by a limb during each step.

$$\boldsymbol{Stepheight} = \|max_{foot_{left}} - min_{foot_{left}}\|\vec{e_z}$$

Based on the positions of the implanted marker set, 3D angles such as flexion & extension, as well as abduction & adduction angles of the hip-, knee- and the foot- joint were derived as described in section 5.

Flexion and extension

Flexion is the movement that decreases the angle between two body parts, involving bending a joint. Extension, on the other hand, increases the angle between body parts, typically involving straightening a joint after flexion.

Abduction and adduction

Abduction is the movement that takes a body part away from the midline of the body. Adduction, on the contrary, brings a body part closer to the midline of the body.

CHAPTER 7

Results

The advancement of the developed gait laboratory entailed multiple workflows. These included a deeper research in animal behavior and the development of a preferred gait system. Additionally they involved the further validation of the implanted marker set by using the scientific rotoscoping approach. The project's primary outcomes were not just the method's establishment and the validation of the X-Ray based mouse gait analysis system's development, but moreover the calculation of certain gait parameters. 3D joint angles were calculated during live locomotion and a pain model was applied to search for gait alterations. Moreover, intra- and inter-individual variations revealed differences in gait and possible reasoning for sample sizes of treatment groups.

7.0.1 Gait system

Before being able to assess locomotion data of female C57BL/6J mice, their behavior and influence of contextual signals on their motor activity was studied through various experimental settings. Factors such as acclimatization time, room lighting, connecting section height, running pattern, apparatus cleaning and testing time were examined.

The results showed that acclimatizing the mice for 1.5 minutes before opening the gate had a greater impact on increasing the frequency of stops compared to immediately opening the gate. Dimmed light conditions resulted in more stops compared to bright lighting. Mice turned around more frequently when the tunnel height was 2.5 inches, but lowering it to 2 inches reduced the number of halts and turns. Allowing mice to run back and forth ten times resulted in fewer stops compared to only letting them run once. Cleaning the apparatus between mouse changes led to more stops compared to no cleaning.

The mice exhibited more activity in the morning (10 am) or evening (5 pm), and walking stability was observed more often at 10 am than at 5 pm. Mice tended to congregate near tunnel entrances and exits and spent increasing time in dark boxes over time. This

experimts conclude that a steady gait was achieved with specific configurations: low environmental impact, lower tunnel height, no cleaning, testing at a less active time, and normal room illumination. Mice were sensitive to environmental influences such as unfamiliar scents and preferred stopping at the ending segment of the tunnel.

Based on these findings, the 16cm field of view was set in the center of the trackway to allow for steady walks and stable outcomes within the limited range of movement illuminated by the X-ray sources. The figure 7.1 below indicates the average stops of the individual mouse (Mouse 1 - 5) at various settings.

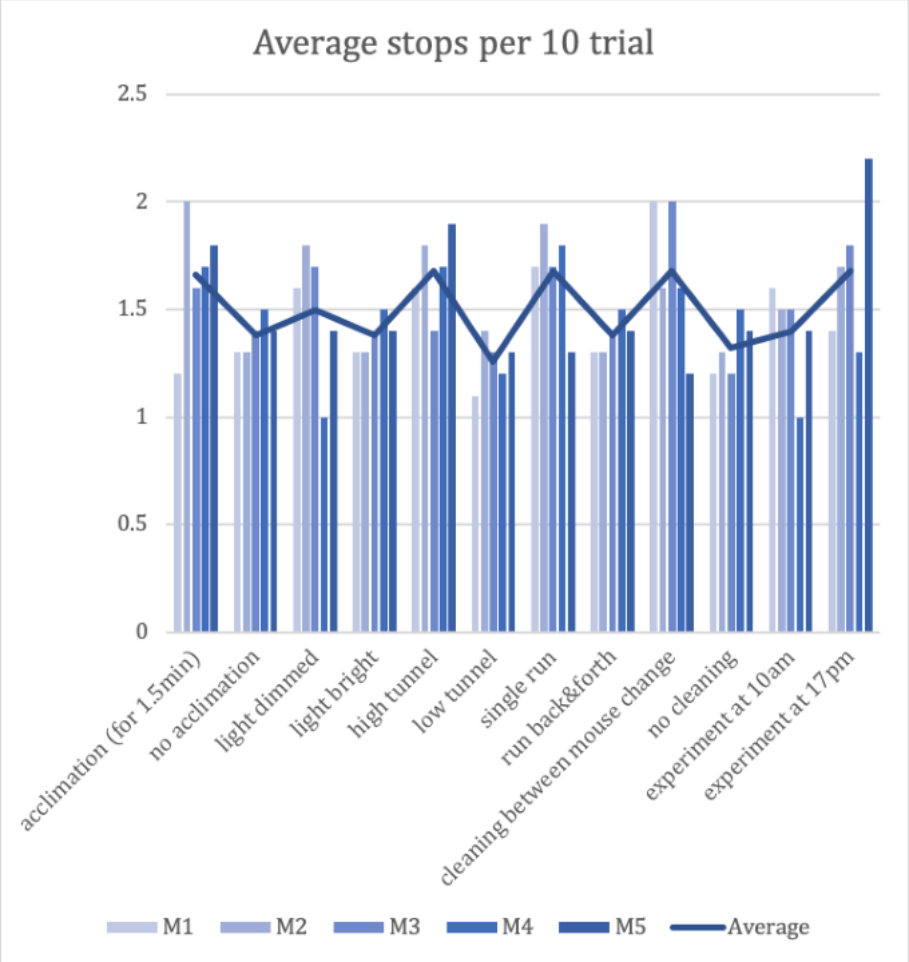

Figure 7.1: Evaluation of uninterrupted locomotion by various experimental settings

7.0.2 SR: movements bone markers and bead markers

The SR workflow was employed to investigate the movement of implanted beads relative to bones during live locomotion in mice. The process involved several steps, including X-Ray video acquisition, marker implantation, recovery period, tracking using μXROMM,

and microCT scanning of the mouse cadaver. The microCT scan of the cadaver generated high-quality DICOM data, which was then used to obtain hindlimb bone objects. The 3D Slicer software was utilized to segment bone mesh models by creating rigid bodies for the pelvis, femur, lower leg, and foot. Areas of interest (ROIs) were manually defined to separate bones and bone markers from soft tissue, while the injected soft tissue marker set was excluded. The bone mesh models were exported as OBJ files, and any artifacts caused by marker beads' radiodensity were smoothed out in Maya without altering the anatomical structure.

The animation and registration process involved generating XYZ marker coordinates in Maya and creating a joint marionette to replicate in-vivo poses. The marionette's hindlimb degrees of freedom were matched independently in every 10th frame, resulting in smooth movement. This registration process aligned the 3D models with the 2D videos.

The subsequent analysis focused on determining the displacement of beads in soft tissue relative to nearby bones. The XYZ coordinates obtained from the μXROMM tracking were imported into Maya, and a "baking" procedure was executed to animate individual objects as if manually animated bone by bone. Marker duplication onto the bones generated a "bone marker set" that remained attached to the bones throughout the locomotion sequence. Two distinct marker sets coexisted: a yellow marker set rigidly attached to the bones and a pink marker set representing the implanted markers exhibiting movement relative to the bones, as seen in 7.2.

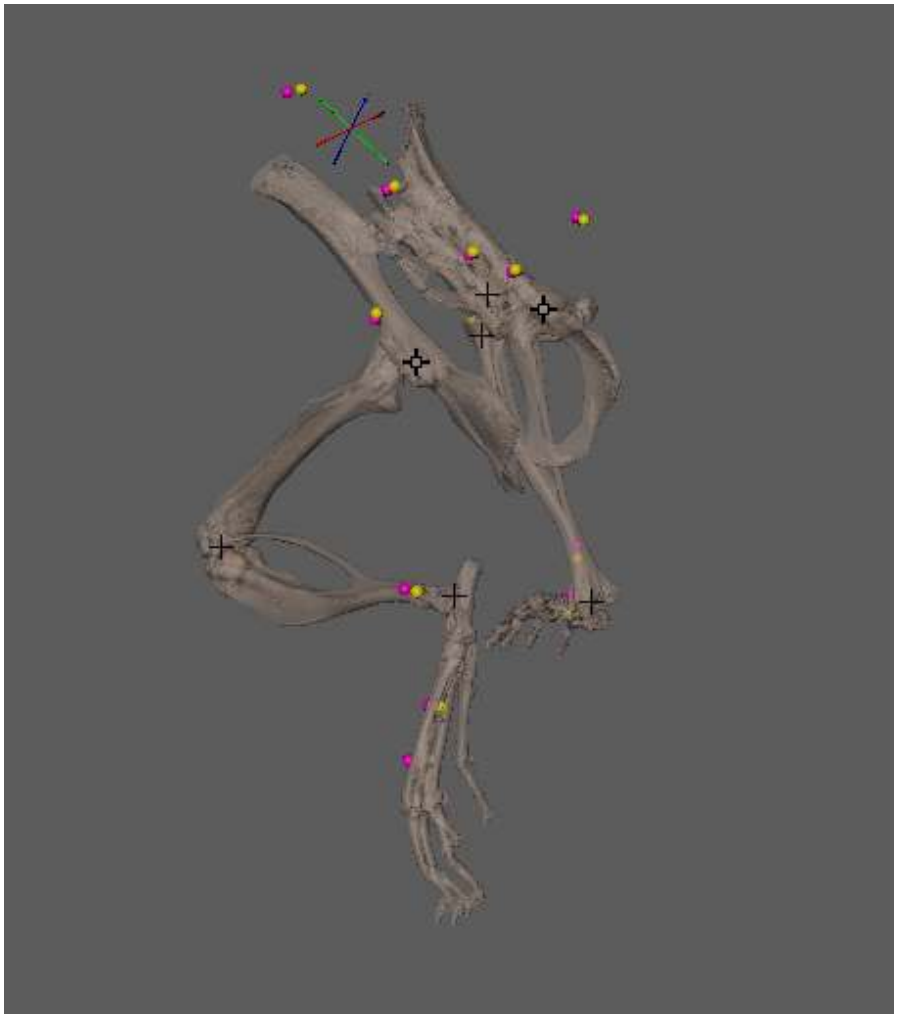

Figure 7.2: Yellow marker set is parented to bone movements, pink marker set are real marker movements

To measure the displacement magnitude between the implanted marker set and the bones, both marker sets were exported, and an Excel file was developed for further analysis.

Figure 7.3 shows the displacement of the implanted marker versus the duplicated marker on the hip joint. The distance was measured using the euclidean distance formula:

$$d\left(p,q\right)=\sqrt{\sum_{i=1}^{n}\left(q_i-p_i\right)^2}$$

The left hip shows a mean distance of $0.17815cm = \ 1.8mm$, and a standard deviation of $0.5mm$.

Figure 7.4 displays the movement of the implanted knee marker to the duplicated marker on the knee joint.

The left knee shows a mean distance of $0.89mm$, and a standard deviation of $0.35mm$.

Similarly, the right hip and the right knee show a mean distance of $1.3mm$ and $0.94mm$ and a standard deviation of $0.36mm$ and $0.32mm$ respectively.

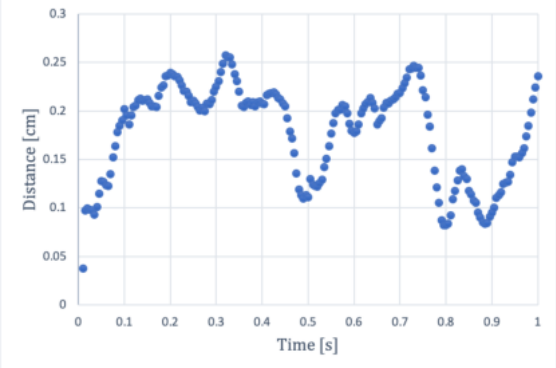

Figure 7.3: Movement of implanted marker to bone marker on left hip

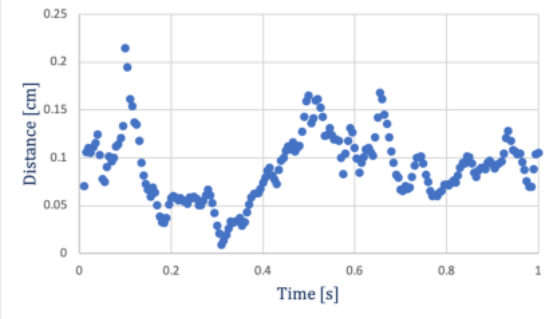

Figure 7.4: Movement of implanted marker to bone marker on left knee

Going into more detail to depict differences of the two marker sets during live locomotion, joint angle calculation were derived using the explained approach in section 5.1.1. When placed in contrast with one another, the two sets of markers reveal distinct variances in their motion. Flexion and extension of the knee is represented in figure 7.5 and is reflected in the minimum and maximum values of each marker set. With a standard deviation of ±6 deg of the left pink knee marker, the left yellow knee marker shares a similar value ±6.7 degrees. The mean flexion / extension angle at the left pink knee marker varied between 139.4 and 108.6 degrees, with a peak to peak distance of 30.7 deg. Similarly, the peak to peak distance of the yellow knee marker is 32.5 degrees.

Figure 7.6 provides a more direct approach to understanding how well the gait laboratory performs in the context of the flexion and extension angle of the left knee. This graph depicts the discrepancy between the actual and bone marker set movements. This was received by subtracting the real marker set movements from the bone marker set movements. The higher noise visible is a result of the noise of two separate measurements being combined through subtraction. This discrepancy, on average, deviates 5.4 degrees from being zero (the pink marker set). Maximum angle of divergence modulus is 9.3 degrees.

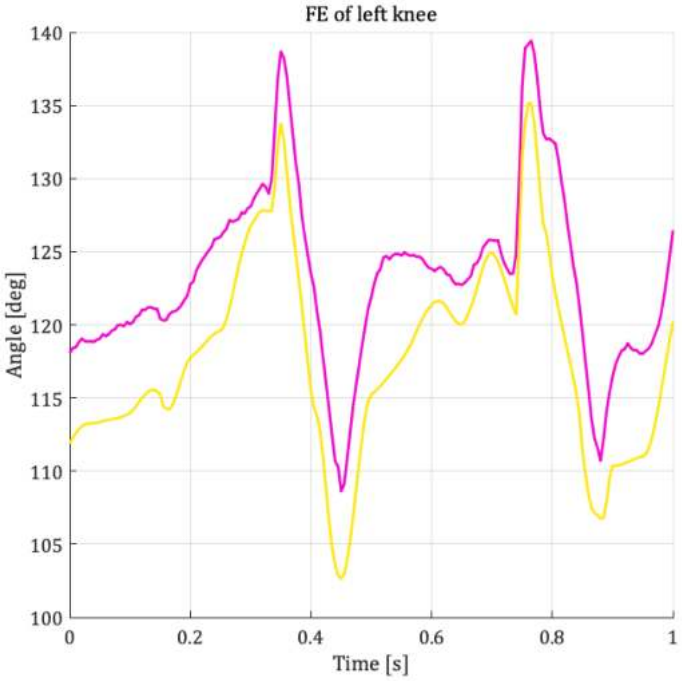

Figure 7.5: Flexion and extension angle of left knee [bone marker set: yellow and real marker set: pink]

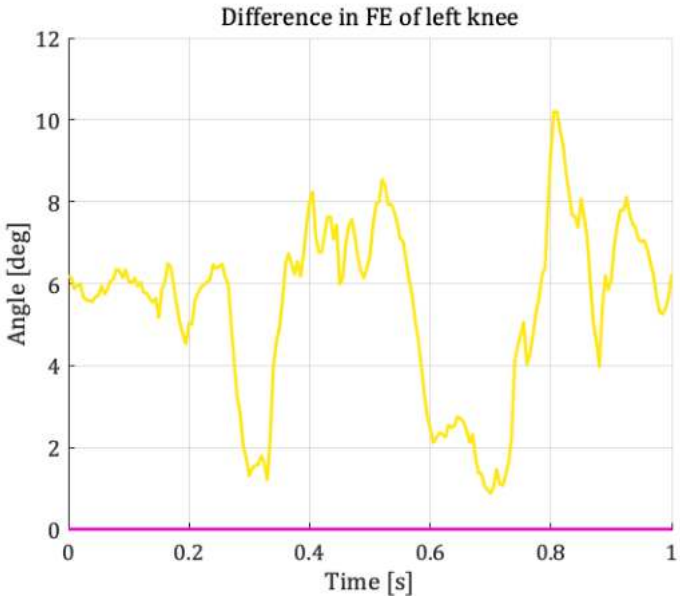

Figure 7.6: Difference of FE angle in left knee of bone marker set to implanted marker set on left knee

Over the same natural locomotion gait cycle, the joint angles flexion & extension and abduction & adduction between the pelvis and femur were also compared between the real marker set to the duplicated bone marker set. Here, the minimum values, representing flexion, are more dissimilar than the maximum ones, signifying extension. The differences in the flexion & extension angles are visualized in figure 7.8. With a standard deviation of ±23.2 deg of the left pink hip marker, the left yellow hip marker shares a similar value ±20.7 degrees. The mean flexion / extension angle at the left pink hip marker varied between 62.8deg and -14.9deg degrees, with a peak to peak distance of 77.7 deg. Similarly, the peak to peak distance of the yellow knee marker is 71.7 degrees. With a mean value of 2.21 degrees, the flexion & extension angles in the hip are overlapping significantly more than in the knee. Once again, this is noticed, when the real marker set (pink) to the bone marker set (yellow) is subtracted.

Figure 7.9 shows the abduction & adduction angle of the left hip. Similar as above mentioned, the real marker set (pink) was subtracted from the bone marker set (yellow) to derive the differences between both marker sets. When compared to the left pink hip marker's ±4.7 degrees of standard deviation, the left yellow hip marker's ±5.2 degrees is quite close. Peak to peak, the average flexion/extension angle at the left pink hip marker was 24.6 degrees, with a range of 33.5 degrees to 8.9 degrees. The graph visually showcases the close alignment of the two marker sets. The peak to peak distance of the yellow hip marker was 22.2 degrees, with a range of 28.7deg to 6.5 deg. Figure 7.10 depicts the discrepancies between both sets. The mean overlapping angle is 3.2 degrees. Maximum peak to peak distance is 12.24 degrees.

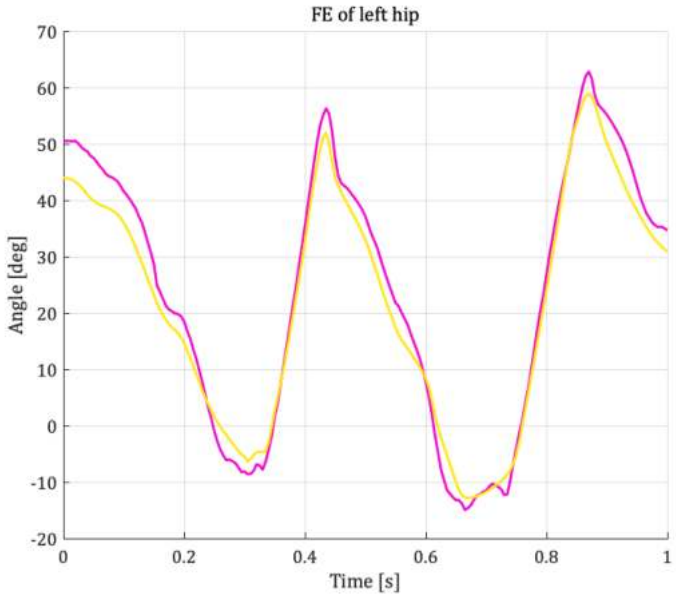

Figure 7.7: Flexion and extension angle of left hip [bone marker set: yellow and real marker set: pink]

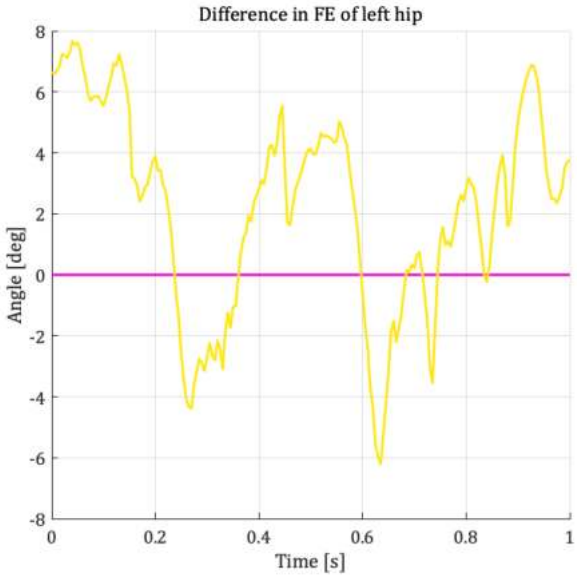

Figure 7.8: Difference of FE angle in left hip of bone marker set to implanted marker set on left knee

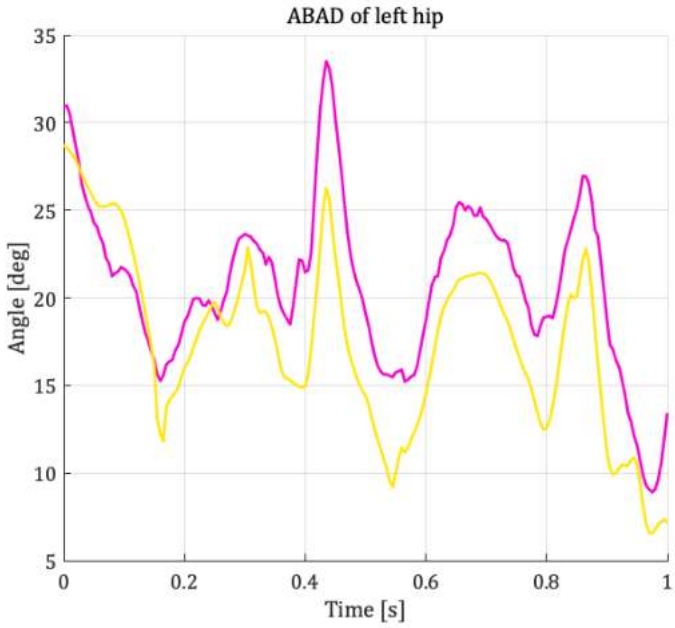

Figure 7.9: Abduction and adduction angle of left hip [bone marker set: yellow and real marker set: pink]

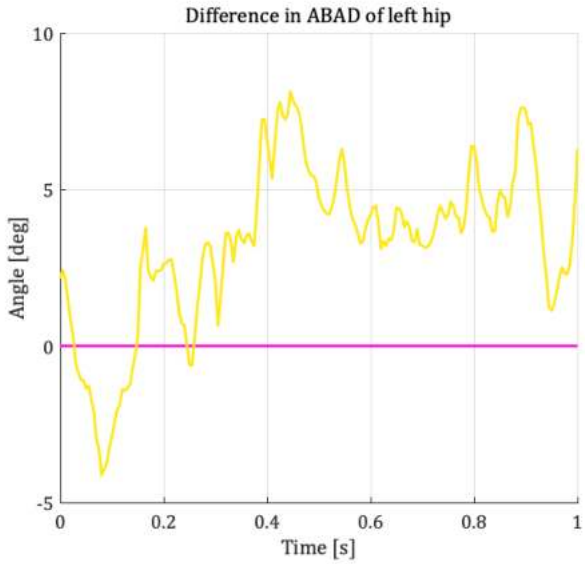

Figure 7.10: Difference of ABAD angle in left hip of bone marker set to implanted marker set on left knee

7.1 Pain model

7.1.1 von Frey

For this thesis, the von Frey method was chosen as the preferred approach for evaluating pain perception. The method was selected due to its simplicity, non-invasiveness, and the ability to facilitate comparisons between different experimental groups. Unlike other invasive techniques that may cause tissue damage or distress to the animals, the von Frey test proved to be a straightforward procedure that could be easily performed with minimal training and equipment. Pain sensitivity was measured using the Ugo Basile® Dynamic Plantar Aesthesiometer 37450. The hind paw's mechanical threshold was measured by exposing the mouse to a metal wire mesh table. The automated testing instrument applied a mechanical stimulus to the hind paw, and the force at which the animal withdrew its paw was recorded. Every mouse was subject of five consecutive trials with sufficient time intervals of 5 minutes between them. The von Frey test revealed that the reaction time required to withdraw the damaged left hind paw decreased by 60% throughout the pain trial. During the pain tests, the average force applied by the metal wire dropped by 56% on average. These results show significant different sensitivity of the injured left hind paw.

Mouse 1		Control	Pain	%Decrease
Left Paw	Reaction Time	5.22	1.4	-73
	Force Intensity	3.08	1.12	-64
Mouse 2		Control	Pain	%Decrease
Left Paw	Reaction Time	5.5	1.1	-80
	Force Intensity	3.18	0.98	-69
Mouse 3		Control	Pain	%Decrease
Left Paw	Reaction Time	4.34	1.84	-58
	Force Intensity	2.52	1.26	-50
Mouse 4		Control	Pain	%Decrease
Left Paw	Reaction Time	4.02	1.7	-58
	Force Intensity	2.34	1.26	-46
Mouse 5		Control	Pain	%Decrease
Left Paw	Reaction Time	2.67	1.04	-61
	Force Intensity	1.97	0.96	-51

Table 7.1: von Frey results of the left paw in control and pain groups

7.1.2 Gait parameters

Stride length

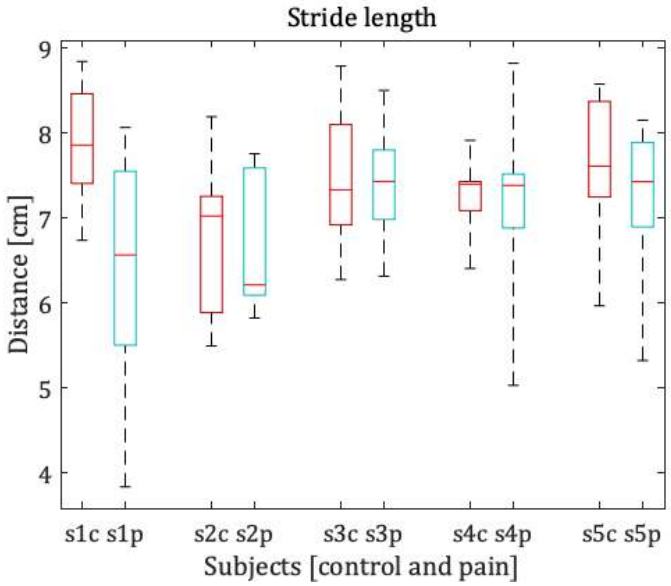

Figure 7.11: Stride length of each mouse [control and pain groups]

After analyzing the stride length of five different mice, each subjected to ten trials, the control results were compared to a pain model group, in which the left hind paw of each mouse had an incision. A t-test was performed to assess the significance of the differences observed. The null hypothesis for the t-test is that the two groups have equal means, while the alternative hypothesis is that the means are unequal. Figure 7.11 shows that for subject 1, the t-test results indicate that there is a significant difference between the pain and control groups (pain vs. control H = 1) with a p-value of 0.009. However, for subjects 2 to 5, the t-test results do not show a significant difference between the groups (pain vs. control H = 0), as the p-values are above the significance level of 0.05.

Step width

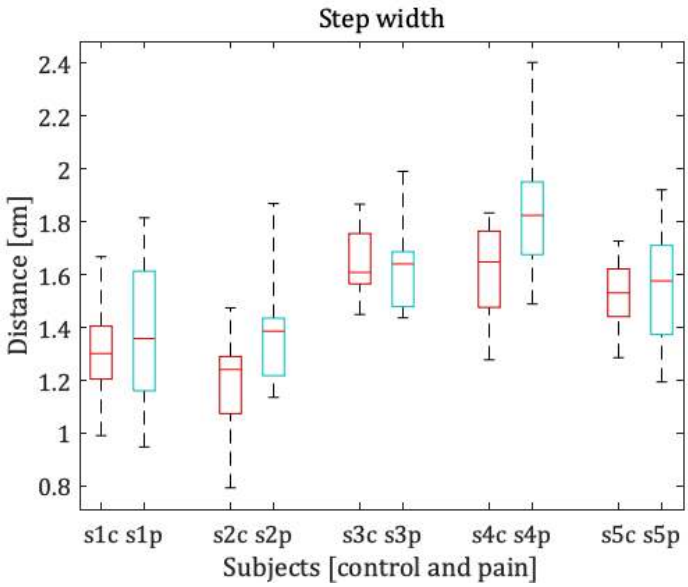

Figure 7.12: Step width of each mouse [control and pain groups]

The parameters used in the t-test for step width analysis are the same as in the step length and stride length analysis. Figure 7.12 shows that for subject 2, the t-test results indicate that there is a significant difference in step width between the pain and control groups (Pain V. Ctl H = 1) with a p-value of 0.044. However, for subjects 1, 3, 4, and 5, the t-test results do not show a significant difference between the groups (Pain V. Ctl H = 0).

Step height

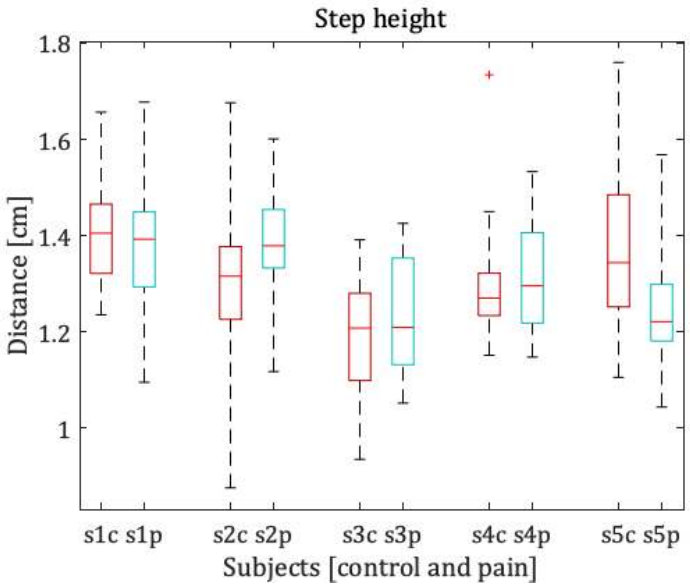

Figure 7.13: Step height of each mouse [control and pain groups]

As to be seen in figure 7.13, for Subject 1, 3 and 4, the t-test indicates that there is no significant difference in step height between the pain and control groups. For Subject 2, the t-test also reveals no significant difference in step height between the pain and control groups. However, the p-value (0.056) is relatively close to the significance level, suggesting a trend towards significance. In contrast, for Subject 5, the t-test yields a significant result. The p-value is 0.011, which is below the significance level. This suggests that there is a statistically significant difference in step height between the pain and control groups for this particular subject.

3D joint angles for left and right limb

The following two figures 7.14 and 7.15 compare the pain group to the control group. The various angle movements, collected by the individual mice are combined. The graphs on the left side showcase the pain model: The red curve symbolizes the mean angles of the left hindlimb with the incised left foot paw and the blue curve symbolizes the mean angles of the right hindlimb. The right side of the figures depict the mean angle movements in the control group. Similarly, the green curve is the mean angle movement of the left hindlimb and the blue depicts the mean value movement of the right hindlimb. All graphs show the mean angles with standard deviation ranges for the left and right side.

The figure 7.14 shows how the results of the 3D angle movements in pain and control groups revealed similar patterns in hip adduction & adduction and flexion & extension movements. When comparing the standard deviation ranges of flexion and extension angles asd depicted in the upper graph between the pain dataset and the control trials, no notable variations emerged. These are ±14.6deg for the left incised hindlimb and ±12.8deg for the right hindlimb in the pain group and ±14.1deg for the left hindlimb and ±13.3deg for the right hindlimb in the control group. Maximum peak values of the left incised hindlimb and the left hindlimb of the control group are similar [41.8deg & 45.2deg]. As well as minimum values of the left hindlimbs [-2deg & 2deg]. Peak to peak variation between incised left hindlimb and control left hindlimb was 0.8 degrees. The mean flexion-extension angle for the right hindlimb at the hip joint varied between 45.3deg and 5.4deg degrees in the pain group and similarly, the mean range in the control group was from 55.5deg to 14.1deg. Peak-to-peak variance between right hindlimb of the pain group and right hindlimb of the control group was 1 degree.

The standard deviation ranges depicted in the lower graph demonstrate striking similarity in the dispersion of hip abduction and adduction angles for both the left and right sides between the pain and the control dataset. With a standard deviation of ±5.8deg of the left incised hindlimb, the left hindlimb from the control group shares a similar value ±5.5deg. The mean abduction-adduction angle at the hip joint in the left incised hindlimb varied between 29.5 and 11.4 degrees. Similarly, the variation of the abad angles in the left hindlimb of the control group was between 28.2 and 12.2 degrees. Peak to peak variation between incised left hindlimb and control left hindlimb was 2 degrees. Equally to the flexion and extension angle, the peak-to-peak variance between right hindlimb of the pain group and right hindlimb of the control group in the abad angle was 1 degree.

The graphs in figure 7.15 reveal a remarkable similarity in the mean flexion and extension angles of knee between the pain- and the control dataset, demonstrating consistent patterns over the measured time period. The standard deviations of the flexion and extension of the knee are ±9.1deg for the left incised limb and ±8.2deg for the left limb in the control group. The mean flexion-extension angle for the right hindlimb at the knee joint varied between 134.5deg and 103.7deg degrees in the pain group and similarly, the mean range in the control group was from 132.3deg to 104.5deg. Peak to peak variance

is 3 degrees. Similarly, the right limb in the pain group (std ±8deg) closely mirrors the right limb in the control group (std 7.15). The right peak to peak variance between pain group and control group is 6 degrees increased.

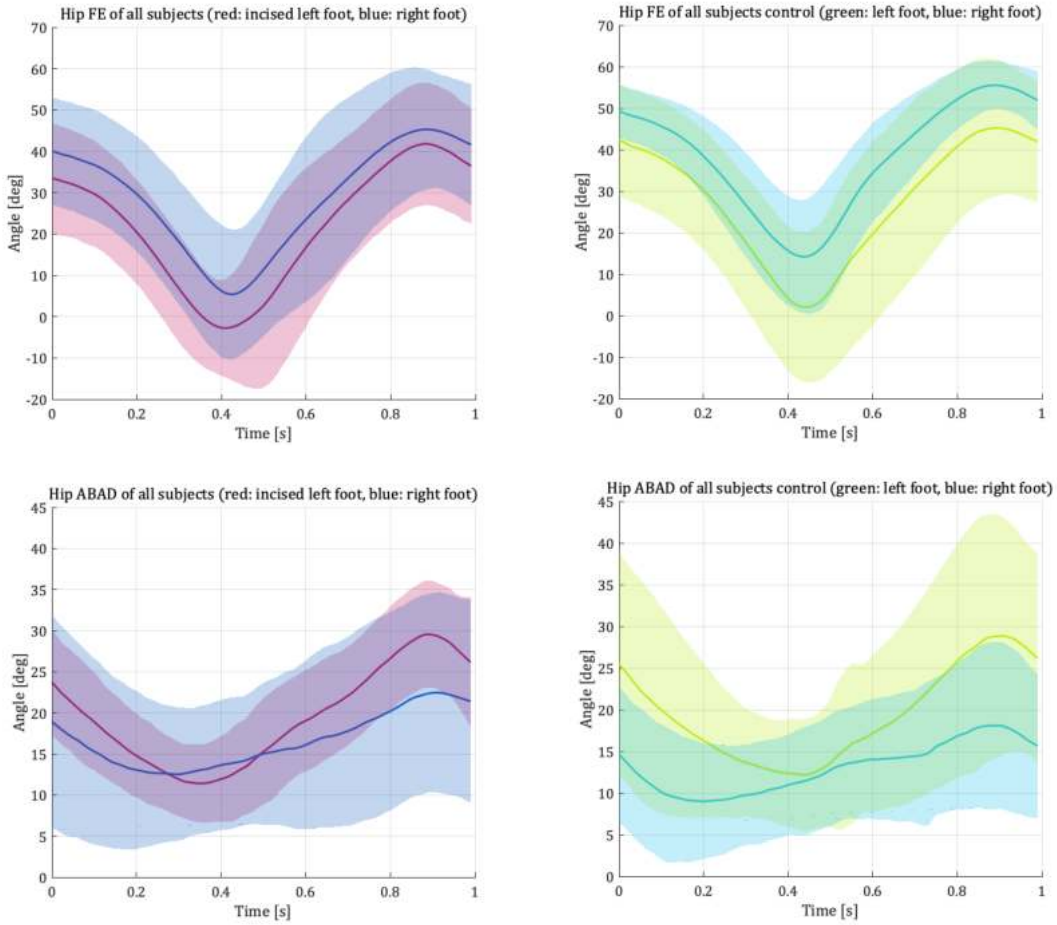

Figure 7.14: FE and ABAD of hip: left and right hindlimb. Pain(left), control(right)

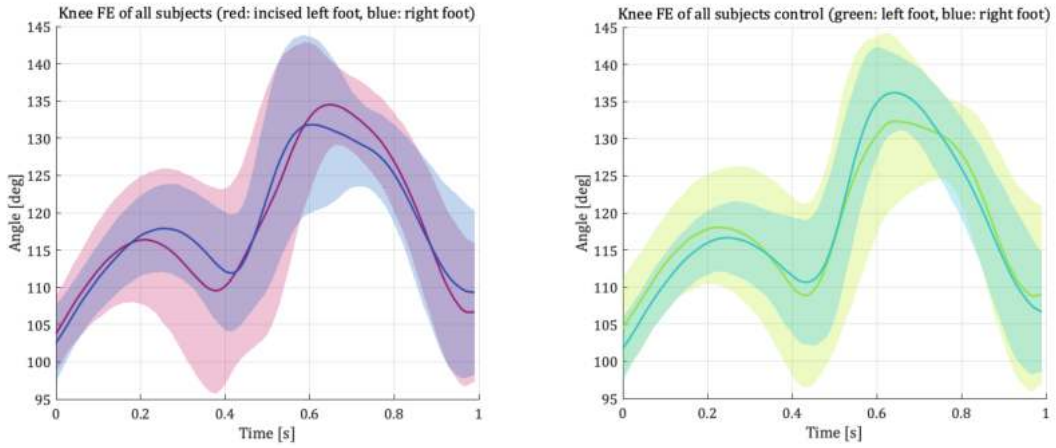

Figure 7.15: FE of knee: left and right hindlimb. Pain(left), control(right)

Spatiotemporal parameters

The limb duty factor and temporal symmetry are spatiotemporal indicators used in gait analysis to assess limb function and detect unilateral limb injuries [Jacobs et al., 2014]. The limb duty factor represents the percentage of time a limb is in ground contact during the gait cycle. On the other hand, temporal symmetry describes the synchronicity of the left-right foot-strike sequence.

$$\text{Limb duty factor} = \frac{\text{stance time of limb}}{\text{stride time of limb}}$$

In rodent gait analysis, limb duty factor and temporal symmetry play crucial roles in identifying unilateral limb injuries. Unilateral gait compensations, such as limping or weight-shifting, are observed in rodents with limb injuries[Jacobs et al., 2014]. These compensations are reflected in the limb duty factor and temporal symmetry measures. For example, if a limb is injured, the duty factor of that limb will decrease, while the duty factor of the contralateral limb will increase.

To analyze the results of limb duty factor, a MATLAB code was employed. The code calculated the limb duty factor for each limb and compared the values between the pain and control conditions. The statistical significance of the differences was assessed using a t-test. The analysis of limb duty factor between pain and control conditions revealed no significant difference across all subjects.

Also the duty factor imbalance was calculated, which represents the difference in duty factor between the left and right limbs. This imbalance can be used to identify unilateral compensations. The output of the written code indicates whether the mean duty factor imbalance was statistically different between the pain and control groups for each subject.

$$\text{duty factor imbalance} = \frac{\text{stance time of left limb}}{\text{stride time of left limb}} - \frac{\text{stance time of right limb}}{\text{stride time of right limb}}$$

Specifically, for Subject 3, there was a significant difference in duty factor imbalance between the pain and control groups (pain versus control H = 1) with a p-value of 0.014. This suggests that for Subject 3, the duty factor imbalance was significantly affected by the presence of pain.

For Subjects 4 and 5, there were also significant differences in duty factor imbalance (Pain V. Ctl H = 1) with p-values of 0.000 and 0.019, respectively. These results indicate that for these specific subjects as well, the duty factor imbalance was significantly influenced by the presence of pain. However, for subject 4 and 5 a controversy in the ttest arises, from the fact that both control and pain groups showed significant differences. P-values of the control group was 0.008 for subject 4 and 0.007 for subject 5.

Similarly, the code analyzed the temporal symmetry measures. It calculated the temporal symmetry for each subject and condition based on the foot-strike sequence. The temporal

symmetry values were then compared between the pain and control conditions using t-tests.

$$\text{Temporal symmetry} = \frac{\text{time of right foot strike} - \text{time of left foot strike}}{\text{stride time}}$$

Based on the formula and the employed t-test, for subject 1, 2, 4, and 5, there was no significant difference in temporal symmetry between the pain and control conditions. However, for subject 3, there was a significant difference with a p-value of 0.020, suggesting that temporal symmetry was altered between the pain and control conditions for this particular subject.

CHAPTER 8

Discussion

For this thesis, a mouse gait laboratory was validated for potential applications in preclinical studies by future collaborators. To receive data from live locomotion, mouse behavior was analysed to gain insight into their gait behavior. The motion of the implanted beats was analysed using a rotoscoping method developed for scientific purposes. A mathematical code was employed to receive information about 3D joint angles. Furthermore, the existing gait laboratory was used in conjunction with a pain model to acquire gait variations.

8.1 Gait system

Observing animal behavior and examining their locomotion on different experimental settings, revealed insights about a gait system that yielded a walking behavior without stopping. A brief period of familiarization with the environment indicated a positive impact on locomotion. The height of the connecting section was crucial, as a reduced height resulted in a reduction in halts and turns, which indicates that a predetermined area of locomotion promotes smoother movements. Motor performance was increased by repeated locomotor activity. Allowing mice to only run a single time resulted in more stops. Interestingly, cleaning the apparatus between mouse changes had a notable impact on the frequency of stops, with more stops observed when cleaning was performed. This indicates that the presence of unfamiliar scents or residual cleaning agents influenced the mice's locomotor behavior, instead of the mouse scent they were used to attributed to housing together with the other mice. The time of day influenced the mice's activity levels and walking stability, with higher activity observed in the morning (10 am) or evening (5 pm). Moreover, walking stability was more frequently observed at 10 am compared to 5 pm, implying diurnal variations in locomotor performance. Additionally, the increasing time spent in dark boxes over time indicates a potential aversion to brightly lit areas or a preference for sheltered environments. The mice exhibited a preference

for congregating near tunnel entrances and exits, suggesting that these areas may hold particular significance for their locomotion. For this reason, the 16cm field of view was placed in the center of the trackway. A steady gait in female C57BL/6J mice can be achieved by considering specific configurations, such as minimizing environmental impact, adopting a lower tunnel height, avoiding apparatus cleaning, conducting tests during less active times, and maintaining normal room illumination.

8.2 SR

The SR workflow successfully tracked and analyzed the displacement of implanted markers in soft tissue relative to nearby bones. This was achieved through a series of steps involving X-Ray video acquisition, marker implantation, recovery period, tracking using μXROMM, and microCT scanning of the mouse cadaver. The 3D Slicer software was employed to segment bone mesh models and create rigid bodies for different skeletal elements, enabling the separation of bones and bone markers from soft tissue. This allowed for accurate tracking and analysis of marker movements in relation to the bones.

The analysis of marker displacement between the implanted marker set and the duplicated marker set attached to the bones provided quantitative measurements of the magnitude of movement. The euclidean distance formula was used to obtain the distances. The results for the mean movement showed 1.8mm$\pm$0.5mm for the left hip and 0.89mm$\pm$0.35mm for the left knee. Due to the fact that the markers were implanted in soft tissues, these results, which are obtained during live locomotion are reasonably small, when set in contrast with the overall movements of joints during locomotion.

Furthermore, joint angle calculations were derived to compare the motion of the two marker sets during live locomotion. First of all, all graphs visually showcase the close alignment of knee flexion and extension, as well as hip flexion and extension and hip abduction and adduction.

The result of the flexion and extension movement of the left pink knee marker showed a peak to peak difference of 30.7 degrees, while the left yellow knee marker was 32.5 degrees. Looking at the hip movement, the similarities between pink and yellow marker set were even more remarkable. From the graphs, it is apparent that the mean hip flexion and extension angles closely mirrors that of the mean hip abduction and adduction angles. With a mean value of 2.21 degrees, the flexion and extension angles of the hip are overlapping significantly more than in the knee.

The small discrepancies observed between the real marker set and the bone marker set can be attributed to various factors, including measurement noise and potential limitations of the tracking and registration process. However, despite these discrepancies, the SR workflow still provides valuable information about the movement patterns and relationships between implanted markers and bones. The results demonstrate that the SR workflow contributes to the validation of the developed gait laboratory. Scientific rotoscoping has the drawbacks of being a time-consuming and laborious process, with variations in results

across and even within operators [Maharaj et al., 2020]. To combat these drawbacks, efforts have been made to automate the procedure for markerless XROMM, as demonstrated by the widespread adoption of the free registration program Autoscoper (Brown University, USA). Unfortunately, such automatic registration systems as Autoscoper are not appropriate for this thesis topic because they have yet to be optimized for multi-bone complexes and very small or overlapping bones [Miranda et al., 2011].

8.3 Pain model

Gait parameters

The analysed gait parameters of the individual mouse show inconsistent effect across individuals in the pain model. The analysis of stride length indicates that there is a significant difference between the pain and control groups only for subject 1. The analysis reveals a significant difference in step width between the pain and control groups only for subject 2, while no significant differences are observed for subjects 1, 3, 4, and 5. The step height shows a significant difference only for subject 5. Overall, the analysis of gait parameters reveals individual variability in the response to the pain model. Some individuals show significant alterations in stride length, step width, or step height, while others do not. This suggests that the impact of pain on gait parameters is not uniform across all subjects and may depend on individual factors. It is possible that the pain model has no effect on gait because there is no consistent effect of these gait factors on the individual mouse in the pain groups. Mice may compensate for the discomfort in their left leg by shifting their weight to their right foot. For this reason, an in depth angle - analysis specifically on the left and right limbs was employed.

3D angle - alterations due to applied pain?

The analysis of 3D joint angles reveals that there are similar patterns in adduction and abduction as well as flexion and extension movements between the pain group and the control group. The standard deviation ranges for these angle movements show no significant variations between the two groups.

The peak values and minimum values of flexion and extension angles in the left hip in both hindlimbs are comparable between the pain group and the control group, with only slight differences observed. The peak-to-peak variations between the incised hindlimb and the control hindlimb are relatively small, indicating consistent movement patterns.

Similarly, the dispersion of hip abduction and adduction angles shows striking similarity between the pain group and the control group, with similar standard deviation ranges observed for both left incised hindlimb and the control hindlimb.

The mean flexion and extension angles of the knee also demonstrate consistent patterns over the measured time period between the pain group and the control group. The standard deviations for these angle movements are relatively close, indicating similar variability in both groups.

Overall, the analysis suggests that the pain group and the control group exhibit similar angle movements in the hip, and knee joints, with only minor differences observed. These findings indicate that the pain model used in the study does not significantly alter the overall movement patterns in the hindlimbs.

Spatiotemporal analysis

The assessment of spatiotemporal parameters is crucial in gait analysis to detect unilateral limb injuries and compensatory mechanisms. The analysis of limb duty factor, which represents the percentage of time a limb is in ground contact during the gait cycle, did not show any significant difference between the pain and control conditions across all subjects. This suggests that the presence of pain did not have a consistent impact on the limb duty factor for the mice in the study.

The duty factor imbalance, which measures the difference in duty factor between the left and right limbs, was used to identify unilateral compensations in the presence of pain. The analysis revealed significant differences in duty factor imbalance between the pain and control groups for subjects 3, 4, and 5. This indicates that the presence of pain led to altered duty factor imbalance in these specific subjects. However, for subjects 4 and 5, it is worth noting that both the pain and control groups showed significant differences, which could suggest other factors influencing the duty factor imbalance.

Temporal Symmetry: The analysis of temporal symmetry, which assesses the synchronicity of the left-right foot-strike sequence, showed no significant difference between the pain and control conditions for subjects 1, 2, 4, and 5. However, for subject 3, there was a significant difference in temporal symmetry between the pain and control conditions. This indicates that the presence of pain affected the temporal symmetry of foot-strike sequence specifically for this subject.

The findings highlight the individual variability in the response to pain-induced alterations in spatiotemporal parameters. While some subjects showed significant differences in duty factor imbalance or temporal symmetry, others did not. This suggests that the impact of pain on these parameters is not consistent across all individuals and may depend on various factors such as pain location, intensity, and individual characteristics.

8.4 Limitations

It is important to acknowledge the limitations of the pain model, including the small sample size and potential confounding factors.

For this study, a sample size of n=5 mice was used. It is possible that insufficient data prevented from seeing clear differences in the pain model's outcomes. The typical sample size for a rodent study is 10-20 animals [Heinzel et al., 2020].

While the von Frey testing as mentioned in 6.2 indicated a robust response from the incised left foot paw to mechanical stimulation, pain could not be reliably detected using

unilateral gait parameter techniques. The lack of statistically significant variations in gait metrics may be due to confounding variables such as the intensity, location, and duration of pain. The nociceptive intensity may also be affected by the time point at which the gait locomotion was recorded.

The controversy observed in the t-test results of the duty factor imbalance 7.1.2 for subjects 4 and 5, where both pain and control groups showed significant differences in duty factor imbalance, raises questions about the interpretation and potential sources of variability in the data.

A fluoroscopy X-Ray system, which would provide higher resolution in locomotion tracking could potentially change this X-Ray based gait analysis. Similar to a study done on rats [Kirkpatrick et al., 2022], the machine learning tool DeepLabCut could be employed to investigate in more accurate locomotion recordings.

To alleviate the difficulties of the time-consuming marker-less XROMM approach (described in further detail in 4.1.2), it could eventually be possible to use the machine learning tool DeepLabCut[Kirkpatrick et al., 2022]. For this approach, a more precise fluoroscopy X-Ray system needs to be employed to allow for more accurate motion tracking.

CHAPTER 9

Conclusion

In conclusion, this thesis successfully validated an X-Ray based mouse gait laboratory for potential applications in preclinical studies. This in-depth project allowed for the analysis of mouse gait behavior and the motion of implanted markers using a rotoscoping method and mathematical code to obtain 3D joint angles. The gait laboratory was utilized in conjunction with a pain model to study gait variations.

The mouse behavior results revealed insights into the locomotion behavior and provided recommendations for achieving a steady gait in female C57BL/6J mice, such as minimizing environmental impact, adopting a lower tunnel height, avoiding apparatus cleaning, conducting tests during less active times, and maintaining normal room illumination.

The SR workflow demonstrated its effectiveness in tracking and analyzing the displacement of implanted markers in soft tissue relative to nearby bones, providing valuable information about the movement patterns and relationships between markers and bones. Despite some discrepancies, the SR workflow contributed to the validation of the gait laboratory.

The analysis of gait parameters and 3D joint angles in the pain model showed similarity and some individual variability in the response to pain-induced alterations. Only few gait parameters exhibited significant differences between the pain and control groups for specific subjects, while an in-depth analysis of joint angles did not. This indicated that the impact of pain was not detected using gait parameters and comparing joint angle movements.

The limitations of the pain model, including the small sample size and potential confounding factors, should be acknowledged. Future studies could explore additional spatiotemporal parameters, consider other factors related to pain, and involve longitudinal studies with larger sample sizes to gain a more comprehensive understanding of the relationship between pain and gait.

Future studies may also collect and analyze locomotion data using a more refined microXROMM system. However, this is contingent on the introduction of advanced X-Ray equipment that is better able to detect soft tissues and thin bones.

Overall, this thesis provides valuable insights into mouse gait analysis, gait variations, and the effects of pain on gait parameters. The validated gait laboratory and the findings contribute to the field of preclinical research and have implications for studying locomotion, interventions, and treatments aimed at enhancing or restoring gait function in mice.

9.0.1 Acronyms

AVI Audio Video Interleave

ABAD Abduction & Adduction Angle

CSV Comma Separated Values

FE Flexion & Extension Angle

IACUC Institutional Animal Care and Use Committee

II Image Intensifier

JPG Joint Photographic Experts Group

kVp Kilovoltage Peak.

microXROMM micro X-ray Reconstruction of Moving Morphology.

OBJ Object File (Wavefront).

ROI Region of Interest.

SD Standard Deviation.

SID Source-Image Distance.

SOD Source-Object Distance.

SR Scientific Rotoscoping.

XMALab X-ray Motion Analysis Lab.

XMAPortal X-ray Motion Analysis Portal.

XROMM X-ray Reconstruction of Moving Morphology

Bibliography

[Bauman and Chang, 2010] Bauman, J. M. and Chang, Y. H. (2010). High-speed X-ray video demonstrates significant skin movement errors with standard optical kinematics during rat locomotion. *Journal of neuroscience methods*, 186(1):18–24.

[Brainerd et al., 2010] Brainerd, E. L., Baier, D. B., Gatesy, S. M., Hedrick, T. L., Metzger, K. A., Gilbert, S. L., and Crisco, J. J. (2010). X-ray reconstruction of moving morphology (XROMM): precision, accuracy and applications in comparative biomechanics research. *Journal of experimental zoology. Part A, Ecological genetics and physiology*, 313(5):262–279.

[Clark et al., 2006] Clark, B. J., Hamilton, D. A., and Whishaw, I. Q. (2006). Motor activity (exploration) and formation of home bases in mice (C57BL/6) influenced by visual and tactile cues: Modification of movement distribution, distance, location, and speed. *Physiology & Behavior*, 87(4):805–816.

[Colville and Bassert, 2016] Colville, T. and Bassert, J. M. (2016). CLINICAL ANATOMY AND PHYSIOLOGY FOR VETERINARY TECHNICIANS, THIRD EDITION. *Elsevier, Ltd.*

[Cook, 1965] Cook, M. J. (1965). The anatomy of the laboratory mouse. *The anatomy of the laboratory mouse.*

[Dorman et al., 2013] Dorman, C. W., Krug, H. E., Frizelle, S. P., Funkenbusch, S., and Mahowald, M. L. (2013). A comparison of DigiGait™ and TreadScan™ imaging systems: assessment of pain using gait analysis in murine monoarthritis. *Journal of pain research*, 7:25–35.

[Gatesy et al., 2010] Gatesy, S. M., Baier, D. B., Jenkins, F. A., and Dial, K. P. (2010). Scientific rotoscoping: a morphology-based method of 3-D motion analysis and visualization. *Journal of experimental zoology. Part A, Ecological genetics and physiology*, 313(5):244–261.

[Golden et al., 2011] Golden, S. A., Covington, H. E., Berton, O., and Russo, S. J. (2011). A standardized protocol for repeated social defeat stress in mice. *Nature Protocols 2011 6:8*, 6(8):1183–1191.

[Heinzel et al., 2020] Heinzel, J., Längle, G., Oberhauser, V., Hausner, T., Kolbenschlag, J., Prahm, C., Grillari, J., and Hercher, D. (2020). Use of the CatWalk gait analysis system to assess functional recovery in rodent models of peripheral nerve injury – a systematic review. *Journal of Neuroscience Methods*, 345.

[Hickman et al., 2017] Hickman, D. L., Johnson, J., Vemulapalli, T. H., Crisler, J. R., and Shepherd, R. (2017). Commonly Used Animal Models. *Principles of Animal Research for Graduate and Undergraduate Students*, pages 117–175.

[Jacobs et al., 2014] Jacobs, B. Y., Kloefkorn, H. E., and Allen, K. D. (2014). Gait Analysis Methods for Rodent Models of Osteoarthritis. *Current Pain and Headache Reports*, 18(10):1–11.

[Kirkpatrick et al., 2022] Kirkpatrick, N. J., Butera, R. J., and Chang, Y.-H. (2022). DeepLabCut increases markerless tracking efficiency in X-ray video analysis of rodent locomotion.

[Knorlein et al., 2016] Knorlein, B. J., Baier, D. B., Gatesy, S. M., Laurence-Chasen, J. D., and Brainerd, E. L. (2016). Validation of XMALab software for marker-based XROMM. *The Journal of experimental biology*, 219(Pt 23):3701–3711.

[Loibl, 2023] Loibl, L. (2023). Development of an X-ray based rodent gait analysis system.

[Maharaj et al., 2020] Maharaj, J. N., Kessler, S., Rainbow, M. J., D'Andrea, S. E., Konow, N., Kelly, L. A., and Lichtwark, G. A. (2020). The Reliability of Foot and Ankle Bone and Joint Kinematics Measured With Biplanar Videoradiography and Manual Scientific Rotoscoping. *Frontiers in Bioengineering and Biotechnology*, 8:500643.

[Mani et al., 2022] Mani, G., Porter, D., Grove, K., Collins, S., Ornberg, A., and Shulfer, R. (2022). A comprehensive review of biological and materials properties of Tantalum and its alloys. *Journal of biomedical materials research. Part A*, 110(6):1291–1306.

[Miranda et al., 2011] Miranda, D. L., Schwartz, J. B., Loomis, A. C., Brainerd, E. L., Fleming, B. C., and Crisco, J. J. (2011). Static and dynamic error of a biplanar videoradiography system using marker-based and markerless tracking techniques. *Journal of biomechanical engineering*, 133(12).

[Modi et al., 2023] Modi, A. D., Parekh, A., and Pancholi, Y. N. (2023). Evaluating pain behaviours: Widely used mechanical and thermal methods in rodents. *Behavioural Brain Research*, 446:114417.

[Monsees et al., 2022] Monsees, A., Voit, K.-M., Wallace, D. J., Sawinski, J., Charyasz, E., Scheffler, K., Macke, J. H., and Kerr, J. N. D. (2022). nature methods Estimation of skeletal kinematics in freely moving rodents. *Nature Methods* /, 19:1500–1509.

[Rizzi et al., 2023] Rizzi, J. S., Almeida, C. d. B., Requena, L. S., Almeida, V. D. d., Mininel, T. V., Silva, G. L. L. d., Oliveira, P. F. d., Júnior, J. d. A. d. C. e. H., Matsumura, C. Y., and Ferretti, R. (2023). Characterization of walking locomotion in aged C57BL/10 mice: a comprehensive gait analysis. *bioRxiv*, page 2023.04.04.535545.

[Schueler, 2000] Schueler, B. A. (2000). The AAPM/RSNA Physics Tutorial for Residents General Overview of Fluoroscopic Imaging1. *https://doi.org/10.1148/radiographics.20.4.g00jl301115*, 20(4):1115–1126.

[Sorge et al., 2014] Sorge, R. E., Martin, L. J., Isbester, K. A., Sotocinal, S. G., Rosen, S., Tuttle, A. H., Wieskopf, J. S., Acland, E. L., Dokova, A., Kadoura, B., Leger, P., Mapplebeck, J. C., McPhail, M., Delaney, A., Wigerblad, G., Schumann, A. P., Quinn, T., Frasnelli, J., Svensson, C. I., Sternberg, W. F., and Mogil, J. S. (2014). Olfactory exposure to males, including men, causes stress and related analgesia in rodents. *Nature Methods 2014 11:6*, 11(6):629–632.

[Wang et al., 2020] Wang, T., Ito, A., Tajino, J., Kuroki, H., and Aoyama, T. (2020). 3D Kinematic Analysis for the Functional Evaluation in the Rat Model of Sciatic Nerve Crush Injury. *Journal of visualized experiments : JoVE*, 2020(156).

[Wong and Shah, 2019] Wong, J. and Shah, P. K. (2019). 3D Kinematic Gait Analysis for Preclinical Studies in Rodents. *Journal of visualized experiments : JoVE*, 2019(150).

[Xu et al., 2019] Xu, Y., Tian, N. X., Bai, Q. Y., Chen, Q., Sun, X. H., and Wang, Y. (2019). Gait Assessment of Pain and Analgesics: Comparison of the DigiGait™ and CatWalk™ Gait Imaging Systems. *Neuroscience Bulletin*, 35(3):401–418.